AD-A257 512

ON PAGE

Form Approved
OMB No. 0704-0188

Public gathe collec Davis

ge 1 hour per response, including the time for reviewing instructions, searching existing data sources. collection of information. Send comments regarding this burden estimate or any other aspect of this ashington Headquarters Services, Directorate for Information Operations and Reports, 1215 Jefferson nagement and Budget, Paperwork Reduction Project (0704-0188), Washington, DC 20503.

1. AGENCY USE ONLY (Leave blank)	2. REPORT DATE 11-13-92	3. REPORT TYPE AND DATES COVERED Annual 10/1/91 - 9/30/92

4. TITLE AND SUBTITLE
Theoretical Analysis of Microwave and Millimeter Wave Integrated Circuits Based on Magnetic Films

5. FUNDING NUMBERS
N00014-89-J-1019
4143115-06

6. AUTHOR(S)
Prof. J.A. Kong

7. PERFORMING ORGANIZATION NAME(S) AND ADDRESS(ES)
Research Laboratory of Electronics
Massachusetts Institute of Technology
77 Massachusetts Avenue
Cambridge, MA 02139

8. PERFORMING ORGANIZATION REPORT NUMBER

9. SPONSORING/MONITORING AGENCY NAME(S) AND ADDRESS(ES)
Office of Naval Research
800 North Quincy Street
Arlington, VA 22217

10. SPONSORING/MONITORING AGENCY REPORT NUMBER

11. SUPPLEMENTARY NOTES
The view, opinions and/or findings contained in this report are those of the author(s) and should not be construed as an official Department of the Army position, policy, or decision, unless so designated by other documentation.

12a. DISTRIBUTION/AVAILABILITY STATEMENT
Approved for public release; distribution unlimited.

12b. DISTRIBUTION CODE

13. ABSTRACT *(Maximum 200 words)*

Work by Prof. Kong and his collaborators is summarized here

92-29774

14. SUBJECT TERMS			15. NUMBER OF PAGES
			16. PRICE CODE
17. SECURITY CLASSIFICATION OF REPORT	18. SECURITY CLASSIFICATION OF THIS PAGE	19. SECURITY CLASSIFICATION OF ABSTRACT	20. LIMITATION OF ABSTRACT
UNCLASSIFIED	UNCLASSIFIED	UNCLASSIFIED	UL

ANNUAL REPORT

Title: THEORETICAL ANALYSIS OF MICROWAVE AND MILLIMETER WAVE INTEGRATED CIRCUITS BASED ON MAGNETIC FILMS

Sponsor by: Department of the Navy
Office of Naval Research

Contract number: N00014-89-J-1019

Research Organization: Center for Electromagnetic Theory and Applications
Research Laboratory of Electronics
Massachusetts Institute of Technology

OSP number: 71387

Principal Investigator: J. A. Kong

Period covered: October 1, 1991 - September 30, 1992

THEORETICAL ANALYSIS OF MICROWAVE AND MILLIMETER WAVE INTEGRATED CIRCUITS BASED ON MAGNETIC FILMS

Under the sponsorship of the ONR Contract Contract N00014–89–J-1019 we have published 29 refereed journal and conference papers.

A macroscopic model is proposed to explain nonlinear electromagnetic phenomena in superconductors. Nonlinear constitutive relations for electromagnetic problems are derived by modifying the linear London's equations. The superelectron number density n_s is a function of the applied current density. The critical current density J_c is derived classically from a critical energy E_c. For temperature $T \neq 0$, the concept of critical current J_c does not imply an abrupt transition of the whole sample from a superconducting state to a normal state when $J > J_c$. A rather smooth variation of $n_s(J)$ is shown instead. The relation, $n_s(J)$, is derived from the Maxwellian distribution of electron velocities at a certain temperature T and a certain macroscopic current density J. Agreement has also been found between this $n_s(J,T)$ model and the temperature dependance of n_s in the two-fluid model. The nonlinear conductivities $\sigma_s(J)$ and $\sigma_n(J)$ are obtained from the London's equation and the $n_s(J)$ function. Nonlinear resistance $R(I)$, kinetic inductance $L_k(I)$ and surface impedance $Z_s(I)$ in thin wire, slab, and strip geometries of superconductors are calculated. A general scheme of solving nonlinear electromagnetic problems in superconductors is proposed. A good agreement between the theory and experiments has been found.

The Riccati differential equation for reflection coefficients in one-dimensional inhomogeneous media is applied to the electromagnetic inverse scattering problem. Two types of Riccati equation in literature, Schelkunoff's and Redheffer's, are derived and distinguished. Based on inverting Redheffer's Riccati equations, both linear and non-linear inversion formulae are proposed. These renormalized perturbation formulae reconstruct the dielectric profile from the reflection coefficient at the surface of the medium. Existing inversion formulae (including the Born approximation) which were obtained from the Green's function approach and the Gel'fand-Levitan-Marchenko (GLM) theory are now

derived from the Riccati equation. Four inversion schemes based on inverting the Riccati equation, linearized Redheffer's Riccati equation, linearized Schelkunoff's Riccati equation, non-linear Redheffer's Riccati equation and non-linear Schelkunoff's Riccati equation approaches, are used to invert several dieletric profiles. Comparison and summary of these methods are given. All these methods give higher order inversion results than the first-order Born approximation. The inversion is performed on band-limited reflection coefficients in frequency domain. An inverse Liouville transform is introduced to rigorously recover the geometric lengths from the stretched coordinates in the inversion procedure.

In general, the inverse methods can be summarized in three categories. The first one is a data base approach. Whenever a measurement result comes in, it will be compared with all the pre-stored patterns in a library to identify the possible targets. In industry, it is called data interpretation which strongly relies on previous experience. The accumulation of data in the library is a learning process. The advantage of this method is that the unknowns can be identified exactly if such target has been seen before so that the cause and the result are directly connected. The disadvantage is that if the data base is not big enough, the target can not be identified, or if the data base is too big, it will take too much time to search for and match the right pattern. The second method is the iterative approach. A forward model of deducing results from cause has been established before the inversion. When a measurement is obtained, a set of guessed values for the unknowns will be put in the forward model as the possible causes. If the predicted result of the forward model does not match the measurement, an adjusted set of parameters will be used as a new guess. The whole procedure will be repeated until the match is found. During iterations, how to correct the error to reach fastest the convergent value is very important. This procedure is also called optimization or error minimization, which by itself is an active research area. Iterative methods are particularly useful when the solution of an integral equation can not be found in an explicit form. As an example of the iterative methods, the Born approximation approximates the forward model in a linearized form, then iterates towards convergence. The advantage of the iterative approach is that an accurate final solution can be found at a relative fast (compare to data base search) speed. The method is also flexible for different kinds of targets, unlike the data base search where the target has to have been seen before. The disadvantage is that the convergence of iteration is not always guaranteed. There are usually more than one minimum of the cost function.

The initial guess is sometimes so critical to assure the right convergent result that *a Priori* information needs to be used. Non-uniqueness is a serious problem in all inversion methods. Sufficient number of measurements are helpful of reducing the degree of non-uniqueness. Formulation of the forward model for the final inversion equation determines how efficient the inversion scheme is, which sometimes also affect the degree of non-uniqueness.

A recently developed inversion method referred to as the renormalized Source-Type Integral Equation (STIE) approach solves the integral equation derived from the Green's function without the linear approximation. The STIE approach formulates an exact forward model, hence is not restricted to low contrast profiles or weak scattering. The STIE method has been applied to profile inversion problems of the soil moisture and oil formation in boreholes, where the medium properties are described by the permittivity and conductivity distributions. The unknown profiles are inverted from the electromagnetic measurements at remote observation points. The third category of inverse methods is the explicit solution approach. When one solves the inversion equation, closed-form solutions may be obtained if the problem is formulated in certain ways and the data is in certain forms. Examples of this method include the Gel'fand-Levitan-Marchenko (GLM) theory when rational reflection coefficient is used and methods of inverting the Riccati equation. The advantage is obviously that the convergence is guaranteed and the speed is excellent. Unfortunately, only a very few practical problems can be solved by using this method. It is usually used as a check for other inversion methods or for mathematical studies. The STIE approach is extended to the case of a general background medium. The formulation of the inversion equation is exact. Numerical optimization methods are employed in the solution of the inversion equation. The inversion equation also has an explicit dependence on the unknowns to be inverted for; this allows one to compute the derivative (including higher orders) of the response with respect to these unknowns in a closed form. Therefore, higher-order convergence can be achieved without increasing much of the computational time. By pre-storing the elements of the inversion equation (which depend only on the background medium and are independent of the unknown profile), the method does not require the solution to the full forward problem repeatedly as in the case of the Distorted Born approach and is therefore faster in implementation. An algorithm is formulated for simultaneously inverting the unknown permittivity and conductivity profiles. As an example, a soil moisture profile is inverted from measurements above the ground.

A full modal analysis is used to study the dispersion characteristics of microstrip lines periodically loaded with crossing strips in a stratified uniaxially anisotropic medium. Dyadic Green's functions in the spectral domain for the multilayered medium in conjunction with the vector Fourier transform (VFT) are used to formulate a coupled set of vector integral equations for the current distribution on the signal line and the crossing strips. Galerkin's procedure is applied to derive the eigenvalue equation for the propagation constant. The effect of anisotropy for both open and shielded stuctures on the stopband properties is investigated.

The input impedance of a microstrip antenna consisting of two circular microstrip disks in a stacked configuration driven by a coaxial probe is investigated. A rigorous analysis is performed using a dyadic Green's function formulation where the mixed boundary value problem is reduced to a set of coupled vector integral equations using the vector Hankel transform. Galerkin's method is employed in the spectral domain where two sets of disk current expansions are used. One set is based on the complete set of orthogonal modes of the magnetic cavity, and the other employs Chebyshev polynomials with the proper edge condition for the disk currents. An additional term is added to the disk current expansion to properly model the current in the vicinity of the probe/disk junction. The input impedance of the stacked microstrip antenna including the probe self-impedance is calculated as a function of the layered parameters and the ratio of the two disk radii. Disk current distributions and radiation patterns are also presented. The calculate results are compared with experimental data and shown to be in good agreement.

The coupled-wave theory is generalized to analyze the diffraction of waves by chiral gratings for arbitrary angles of incidence and polarizations. Numerical results for the Stokes parameters of diffracted Floquet modes versus the thickness of chiral gratings with various chiralities are calculated. Both horizontal and vertical incidences are considered for illustration. The diffracted waves from chiral gratings are in general elliptically polarized; and in some particular instances, it is possible for chiral gratings to convert a linearly polarized incident field into two nearly circularly polarized Floquet modes propagating in different directions.

A general spectral domain formulation to the problem of radiation of arbitrary distribution of sources embedded in a horizontally stratified arbitrary magnetized linear plasma is presented. The fields are obtained in terms of electric and magnetic type dyadic Green's functions. The formulation is considerably simplified by using the kDB system of coordinates in conjunction with the Fourier transform. The distributional singular behavior of the various dyadic Green's functions in the source region is investigated and taken into account by extracting the delta function singularities. Finally, the fields in any arbitrary layer are obtained in terms of appropriately defined global upward and downward reflection and transmission matrices.

We have investigated a method for the calculation of the current distribution, resistance, and inductance matrices for a system of coupled superconducting transmission lines having finite rectangular cross section. These calculation allow accurate characterization of both high-T_c and low-T_c superconducting strip transmission lines. For a single stripline geometry with finite ground planes, the current distribution, resistance, inductance, and kinetic inductance are calculated as a function of the penetration depth for various film thickness. These calculations are then used to determine the penetration depth for Nb, NbN, and $YBa_2Cu_3O_{7-x}$ superconducting thin films from the measured temperature dependence of the resonant frequency of a stripline resonator. The calculations are also used to convert measured temperature dependence of the quality factor to the intrinsic surface resistance as a function of temperature for a Nb stripline resonator.

Proximity-print x-ray lithography is commonly performed with gold or tungsten structures of sizes down to 30 nm wide and 50–800 nm tall which are patterned onto the surface of a thin, x-ray transparent membrane. X-rays in the wavelength range of 0.5–5 nm are used for replication with mask-substrate gaps ranging from zero (contact print) up to 20 μm or more. The resolution o f this method (minimum achievable linewidth) is limited predominantly by the diffraction of the x-rays *around* these structures and the spreading of the diffracted waves *into* the 0–20 μm gap. Work to date has assumed that scalar diffraction theory is applicable—as calculated, for example, by the Rayleigh-Sommerfeld formulation—and that Kirchhoff boundary conditions can be applied. Kirchhoff boundary conditions assume that the fields are constant in the region between the absorbers, and also (a different) constant in the region just under the absorbers, and that there are no fringing fields. In this report we explore the validity of this assumption for the case

of 30 nm-wide by 30–100 nm-tall gold absorbers with 4.5 nm (C_K) x-rays. Because of computational time limitations, the shorter wavelength and larger absorber cases are not currently possible.) Because the absorber is only 7 wavelengths wide and 7–20 wavelengths high, strong diffractive effects are expected. The finite-difference time-domain (FD-TD) technique was used on a Cray-2 supercomputer to predict the fields diffracted by the gold absorbers. In applying the FD-TD technique, Maxwell's equations are discretized in space and time on a uniform rectangular grid. A second-order absorbing boundary condition is applied at the outer boundary of the computational domain in order to simulate unbounded space. The results indicate that strong fringing fields exist in the shadow region of the absorber, and hence Kirchhoff boundary conditions are not accurate in this regime.

Because the effects of diffraction during proximity-print x-ray lithography are of critical importance, a number of previous researchers have attempted to calculate the diffraction patterns and minimum achievable feature sizes as a function of wavelength and gap. Work to date has assumed that scalar diffraction theory is applicable–as calculated, for example, by the Rayleigh-Sommerfeld formulation–and that Kirchhoff boundary conditions can be applied. Kirchhoff boundary conditions assume that the fields (amplitude and phase) are constant in the open regions between absorbers, and a different constant in regions just under the absorbers (i.e., that there are no fringing fields). An x-ray absorber is, however, best described as a lossy dielectric that is tens or hundreds of wavelengths tall, and hence Kirchhoff boundary conditions are unsuitable. In this report we use two numerical techniques to calculate (on a Cray 2 supercomputer) accurate diffracted fields from gold absorbers for two cases: a 30 nm-wide line at $\lambda = 4.5$ nm, and a 100 nm-wide line at $\lambda = 1.3$ nm. We show that the use of Kirchhoff boundary conditions introduces unphysically high spatial frequencies into the diffracted fields. The suppression of these frequencies–which occurs naturally without the need to introduce an extended source or broad spectrum–improves exposure latitude for mask features near 0.1 μm and below.

In order to understand the physical meaning of rational reflection coefficients in one-dimensional inverse scattering theory for optical waveguide design, we have studied the relation between the poles of the transverse reflection coefficient and the modes in inhomogeneous dielectrics. By using a stratified medium model it is shown that these poles of the reflection coefficient have a one-to-one correspondence to the discrete modes, which are the guided and leaky modes. The radiation modes have continuous real values of transverse wave numbers and are not represented by the poles of the reflection coefficient. Based on these results, applications of the Gel'fand-Levitan-Marchenko theory to optical waveguide synthesis with the rational function representation of the transverse reflection coefficient are discussed.

We developed an inversion algorithm based on a recently developed inversion method referred to as the Renormalized Source-Type Integral Equation approach. The objective of this method is to overcome some of the limitations and difficulties of the iterative Born technique. It recasts the inversion, which is nonlinear in nature, in terms of the solution of a set of linear equations; however, the final inversion equation is still nonlinear. The derived inversion equation is an exact equation which sums up the iterative Neuman (or Born) series in a closed form and; thus, is a valid representation even in the case when the Born series diverges; hence, the name *Renormalized* Source-Type Integral Equation Approach.

The scattering and receiving characteristics of a probe-fed stacked circular microstrip antenna, both as an isolated element and in an infinite array, are investigated.

The receiving case, where the antenna is loaded with impedance Z_L, is solved by superposition, decomposing the problem into the scattering case with $Z_L = 0$ and the transmitting case. In the scattering case, the coaxial probe is short-circuited to the ground plane and the induced probe current I_1 due to an incident plane wave excitation is determined. In the transmitting case, a voltage V is applied to the base of the probe and the input impedance Z_{in} is solved for, giving a relationship between the applied voltage V and the transmitting probe current I_2. With the knowledge of I_1 and Z_{in}, for a given load impedance Z_L, the total probe current, $I = I_1 + I_2$, and the received power are determined.

The scattering and transmitting problems are solved rigorously using a dyadic Green's function formulation where the mixed boundary value problem is reduced to a set of coupled vector integral equations for the unknown disk and probe currents. Galerkin's method is employed in the spectral domain where the disk current distributions are expanded in terms of the complete set of transverse magnetic (TM) and transverse electric (TE) modes of a cylindrical resonant cavity with magnetic side walls. An additional term is added to the disk current expansion to properly model the singular behavior of the current in the vicinity of the probe, to ensure continuity of the current at the probe/disk junction, and to speed up the convergence of the solution.

The radar cross section (RCS) of a single stacked microstrip antenna is calculated for both the open and short-circuited cases. For an infinite array of phased elements, the reflection coefficient seen at the input of the antenna and the received power are calculated.

The complex resonant frequencies of the open structure of a microstrip antenna consisting of two circular microstrip disks in a three layer stacked configuration have been rigorously calculated as a function of the layered parameters and the ratio of the radii of the two disks. Using a dyadic Green's function formulation for horizontally stratified media and the vector Hankel transform, the mixed boundary value problem is reduced to a set of coupled vector integral equations. Employing Galerkin's method in the spectral domain, the complex resonant frequencies are calculated and convergence of the results is demonstrated. It is shown that for each mode, the stacked circular microstrip structure has dual resonant frequencies which are associated with the two coupled constitutive resonators of the structure and which are a function of the mutual coupling between them. This mutal coupling depends on the geometrical configuration of the stacked structure, the layered parameters, and the disk radii. The maximum coupling effect occurs where the real parts of the resonant frequencies of the constitutive resonators are approximately equal, where the behavior of the resonances in this region is a function of the coupling. The dual frequency behavior of the stacked microstrip structure, easily controlled by varying the parameters of layer 2 and disk radii ratio, given fixed parameters for layer 1 and layer 3, may be used to broaden the bandwidth or provide for dual frequency use of the antenna.

We rigorously analyze the radiation problem of a circular patch which is center fed by a coaxial-line driven probe over a ground plane and situated in an arbitrary layered medium. The current distribution on both the patch and the probe is rigorously formulated using a planar stratified medium approach. A set of three coupled integral equation is derived which governs the axial current distribution on the probe, the radial current distribution on the patch and the azimuthal magnetic current sheet across the aperture of the driving coaxial line. This set of equations is then solved using the method of moments. The resulting matrix equation is obtained in terms of Sommerfeld-type integrals that take into account the effect of the layered medium. These integrals are efficiently computed by a simple deformation in the complex wavenumber domain. The probe current distribution, input impedance and radiation pattern are presented and compared to the case of a uniform probe current distribution.

Microstrip antennas of stacked configurations have received attention in recent years for both wideband and dual frequency use, overcoming the narrow bandwidth of conventional single layer microstrip antennas. Although much experimental work has been performed, theoretical analyses of stacked microstrip patches is limited. Resonant frequencies of the stacked microstrip antennas have been rigorously calculated. Numerical methods have been used to calculate the current and radiation fields of a stacked microstrip antenna. The method of moments has been applied to analyze to the stacked microstrip structure when excited by an incident plane wave. A spectral domain iterative analysis for a stacked microstrip antenna where the antenna is described by a rectangular sampling grid has been used to calculate radiation patterns. This analysis does not allow for accurate modeling of the probe feed.

In our approach, the input impedance and radiation fields of a coaxial probe-fed microstrip antenna consisting of two circular microstrip disks in a stacked configuration are investigated. Using a dyadic Green's formulation, a rigorous analysis of the microstrip antenna is performed for two stacked configurations. Assuming uniform current along the probe, the mixed boundary value problem is reduced to a set of coupled vector integral equations using the vector Hankel transform and solved using Galerkin's method in the spectral domain. Due to the singular nature of the current on the driven disk in the vicinity of the probe, an additional term is included in the current expansion to account for the

divergent nature of the current near the probe feed junction and insure continuity of the current at the junction.

The input impedance and radiation patterns of the stacked microstrip antenna is calculated as a function of the layered substrate, permittivities and thicknesses, and the ratio of the radii of the two disks. Both dual frequency and wideband operation is discussed.

Microstrip discontinuities, such as open end, gap and step in width, have been widely studied by many authors. There are different methods for analyzing microstrip discontinuities, such as quasi-static approach, planar waveguide model and integral equation formulation. As the frequrncy gets higher, the quasi-static assumption is not valid. In the planar waveguide model analyses, the thickness of the substrate is assumed much smaller than the wavelength so that a two-dimensional model may be applied. In this case, the effect of the radiation and the surface waves are not considered. The integral equation method has been applied to study the open end and gap dicontinuities on isotropic substrates. In applying the integral equation method, various approximation were introduced in the computation procedure. More recently, finite element expansion currents are used to formulate a full-wave analysis of micristrip discontinuities on isotropic substrates.

The open end, gap and step in width discontinuities placed on anisotropic substrates are rigorously analyzed. Both uniaxial and tilted uniaxial anisotropy are considered. The materials are assumed to be lossless and the metal strips to be infinitely thin. A dyadic Green's function for layered anisotropic media is used to formulate a set of vector integral equations for the current distribution. The fundamental hybrid mode is assumed to be propagating on the input and output of microstrip lines. In solving the set of vector integral equations, the method of moment is employed. The basis functions for the current on the metal strip consider the edge effect. Both logitudinal and transverse currents are considered in the calculation. The propagation constant for the infinitely long uniform microstrip line is first calculated. Then the propagation constant of the fundamental mode is used to formulate the excitation of the discontinuity problem. At the discontinuity, local basis functions are used to simulate the local currents near the discontinuity. The scattering matrix can then be obtained, and an equivalent circuit model can be proposed. The effect of the anisotropy is investigated and the results are discussed.

The leakage phenomenon is important in the area of millimeter-wave integrated circuits and integrated optics. Theoretical analyses and experiments have been performed to investigate this phenomenon. The leakage is due to the TE-TM coupling occurring at the geometrical discontinuities, and the leaky power in the form of surface wave propagates in the background medium.

There are different methods to analyze the dielectric strip waveguides, including the approximate field matching method, effective dielectric constant (EDC) method, mode matching method, etc. The first two methods are approximate, and can not be used to predict the imaginary part of the propagation constant. In the third one, ground planes have to be put at some distance away from the guiding structure, hence the effect of radiation loss is neglected.

An integral equation formulation using dyadic Green's function is derived to solve for the dispersion relation of single and coupled dielectric strip waveguides. A method to predict the leakage is presented, and the leakage properties are investigated.

Three different dielectric strip waveguides are investigated : optical rib waveguide, strip dielectric guide, and insulated image guide. Both single and coupled strip waveguides are studied. The cross section of the dielectric strips are assumed to have rectangular shape. Applying the Galerkin's method, the field distribution on the cross section are represented by a set of unit pulse basis functions. Substituting these basis functions into the integral equations, and choosing the same set of basis functions as the testing functions, we can obtain a determinant equation from which the propagation constant can be solved.

For single dielectric strip waveguide, it is observed that the leakage occurs when the effective refractive index is smaller than that of a surface wave mode in the background medium. It is also observed that if the lowest TE-like (TM-like) mode is leaky, the lowest TM-like (TE-like) mode is non-leaky. When the lowest order mode leaks, the surface wave mode of opposite polarization is excited. When the higher order mode leaks, the surface wave modes of both polarizations can be excited.

For two symmetrical dielectric strip waveguides, both the even and odd modes are investigated. For the leaky mode, the total leakage is due to the leakage from each individual strip waveguide. At the separation where the even mode has a maximum leakage, it implies that the surface wave modes excited by each waveguide add in phase. For the odd mode at about the same separation, these coaxial line feed, the reflection coefficient for the TEM mode is obtained which allows one to compute the input impedance at the terminals of the probe. Numerical results for the input impedance are presented.

A finite difference time domain technique for two dimensional time domain scattering of electromagnetic waves is derived. The triangular grids and the control region approximation are employed to discretize Maxwell's equations. The finite difference time domain techniques with uniform rectangular grids has been used in the past. The scatterers are modeled using staircases and, recently, the accuracy of this approximation has been investigated. Several types of other grids have been proposed to improve the staircase approximation. Generalized nonorthogonal grid can model scatterer without staircasing. It has been applied to spherical systems, yet they appear to be cumbersome for general scatterers. The "distorted rectangular grid" model approximates the computational domain using rectangular grids and distorts the boundary grids to fit the interfaces. The triangular grid is used in this paper, which is very flexible in dealing with arbitrary scatterers and absorbing boundaries.

The control region approximation, which calls for Delaunay and Dirichlet tessellation, has been successfully applied to the frequency domain problems in the past. Two double integral terms are obtained by integrating the Helmholtz equation about the Delaunay tessellation. The term involving the Laplace operator can be converted to a closed loop integral of normal derivatives, which can easily be approximated in finite difference manner by utilizing the orthogonal property of Delaunay and Dirichlet tessellation. The remaining term can be approximated by multiplying the field at the node with the area. In the time domain problem, the same approximation is applied to the wave equation, except the term involving time derivatives is used in time marching scheme. Alternatively, as in Yee's algorithm, the first order Maxwell's equations are solved by spatially and temporally separating the electric and magnetic fields. In the case of electric polarization, the electric fields are placed at the nodes and the magnetic fields are placed at the center of triangular edges. The curl H equation is integrated by applying Stoke's theorem and convert it to a

closed loop integral of tangential magnetic fields. This equation can be used to advance electric fields in time. To update magnetic fields, the second curl equation is used. This equation is approximated in the finite difference manner by utilizing the orthogonality property of the tessellation. The equations for the magnetic polarization case can also be derived following the similar procedure.

In order to limit the computation domain, the scatterers are enclosed with artificial outer boundaries. Continuous smooth outer boundaries, such as circles and ellipses, are chosen. The second-order time domain absorbing boundary conditions derived from the pseudo-differential operator approach is imposed at the outer boundaries. These boundary conditions are implemented with the control region approximation to determine necessary field quantities at the boundary. The results of the time domain control region approach are presented for simple scatterer geometries, such as conducting and coated cylinders and strips, by calculating both the transient and time-harmonic responses.

The Finite-Difference Time-Domain (FD-TD) method was first introduced by Yee who discretized Maxwell's time dependent curl equations with second-order accurate central-difference approximations in both the space and time derivatives. Since then, it has been applied extensively to scattering and wave absorption problems. Application of the FD-TD method to microstrip problems, in which frequency-domain approaches have dominated, has so far attracted little attention until recently it was used to obtain frequency characteristics of microstrip cavities. Also, it has been extended to the analyses of open microstrip line and microstrip discontinuity problems where absorbing boundary conditions are needed for the simulation of the unbounded domain. However, only isotropic or simple anisotropic media are considered in the above papers.

A new FD-TD grid model is used to solve microstrip problems in anisotropic media having tilted optical axes expressed by permittivity or permeability tensor with off-diagonal elements. This grid model is indeed a superposition of two conventional grids with some displacement which depends on the optical axes of anisotropy. Implementations of different boundary conditions are discussed. Using this model, the frequency-dependent characteristics of microstrip lines are investigated. The microstrips are assumed to be placed on top of anisotropic substrates with tilted optical axes. The case with superstrates is also investigated.

In the finite difference computation, the open-end termination is simulated by using the open-circuit, short-circuit technique. The source plane is implemented by using a magnetic wall with a Gaussian pulse excited on the surface under the strip. Because of the symmetry of the problem, the region under consideration can be reduced by half, using a magnetic-wall at the center plane.

The fields at different positions are first calulated. Then the Fourier Transform is taken to give the field spectra from which the voltage and current can also be obtained. Using these data, the effective permittivity and the characteristic impedance can be determined. The frequency characteristics of microstrip lines in anisotropic media obtained by this method are compared with the published results.

Finite difference time domain (FDTD) techniques show great promise in their ability to solve three dimensional problems with arbitrary geometry. Advantages of this method include the ability to model spatially or temporally varying media. These advantages are due to the complete discretization of both space and time. Considering the volume of information being calculated these techniques are very efficient and are well suited to calculation on future parallel processing computers. This method was first formulated by Yee in 1966 and his basic algorithm is still in use. Recent work has demonstrated the applicability of the FDTD technique to microstrip problems. The centered finite difference approximations used are second order accurate in both space and time yielding good results for reasonable mesh sizes. Numerical techniques used to solve electromagnetic problems must limit the domain over which the fields are to be calculated. This mandates the use of an absorbing boundary condition to simulate the outward propagation of waves incident on the walls of the mesh. An absorbing boundary condition has been developed by Mur based on the work of Enquist and Majda.

Our work in this area includes development of the algorithms mentioned above into a general purpose computer code which may be used to solve for the transient response of electromagnetic problems with an arbitrary geometry. In addition to the transient response, frequency domain parameters may be obtained by fourier transform of the time domain results. Since the fields are calculated throughout space and time all other desired parameters may be calculated from the field quantities. Specifically, we are analyzing rectangular microstrip structures with as many as two or more ports. Such structures may be used in MMIC filters or antennas. This problem is of interest for several reasons. First, there are existing frequency domain solutions to the resonance problem of a rectangular microstrip patch, which we may compare with the FDTD solution. Secondly, the FDTD technique may be used to analyze coupling of microstrip lines to the rectangular structure. This coupling may be either a direct connection or a gap coupled connection. Advantages of the FDTD solution of this problem are that it is a full wave solution which allows for radiation or surface wave loss and that no empirical values such as "effective" dimensions are needed for the analysis, also the geometry may be altered easily to allow for various connections or coupling to the patch. This is a significant improvement over methods which rely on a planar circuit approach in which the substrate thickness must be small compared to wavelength and inherently three dimensional coupling problems are not easily handled. Comparison of our results with various planar circuit approaches will be made.

A new perturbation series, coupled integral equation approach for calculating the frequency dependent circuit parameters for quasi-TEM transmission lines with lossy conductors is presented. The method considers the addition of loss and dispersion to be perturbations on the lossless TEM case, and therefore the difference between the propagation constant and the wavenumber in free space is a small parameter. We obtain the lowest order term of the perturbation series by solving two quasistatic problems; the electrostatic problem to get the capacitance, and the magnetoquasistatic problem, with the distribution of current inside the wire considered, which gives the frequency-dependent inductance and resistance. Both of these problems are solved using one-dimensional integral equations for quantities on the surface of the conductor; this represents a significant improvement in efficiency over previous methods. For most cases of practical interest, the lowest order term of the series will suffice. If, however, the change in the propagation constant from the

lossless case, due to the altered inductance and the addition of resistance, is significant, additional terms in the perturbation series can be calculated.

The method is illustrated with the case of one or more wires embedded in a uniform dielectric. In the original magnetoquasistatic problem, the current is entirely directed along the axis of propagation, and satisfies the frequency-domain diffusion equation. Outside the wire, the magnetic vector potential is in the same direction, and obeys Laplace's equation. The boundary conditions are the continuity of tangential and normal magnetic field at the interface, which can be expressed in terms of the current density and vector potential and their derivatives. Since we can express the ratio of the frequency-dependent resistance to the DC resistance in terms of the values of the volume current and its normal derivative on the surface of the wire only, we can use a pair of coupled integral equations to solve for these quantities alone, which we can solve by Galerkin's method or other finite element methods.

Results obtained using this technique are shown for some important cases, including rectangular wires, and are compared with earlier methods and with experimental data. Previous methods for calculating the resistance fall into three categories. First, for certain cases, exact analytical results can be obtained. Secondly, especially in the case of a rectangular wire, the cross-section can be divided into rectangular segments, each much smaller than a skin-depth, across which the current is assumed to be constant. Magnetoquasistatics gives simple answers for the resistance and self-inductance of each element, and the mutual inductance between elements. This leads to a matrix equation which is solved for the current distribution. The disadvantages of this technique are that it requires basis functions throughout the cross-section of the conductor, which is especially intensive as the frequency gets large. Also, closed form expressions for the matrix elements only exist when the elements are rectangular — other shapes, such as triangular patches, which might be used to fit a wire of arbitrary shape, lead to nested numerical integrals.

The third method used is a variational procedure. This is similar to the method presented here, except that the current and the magnetic vector potential are expanded in functions which span the entire cross-section. This has two drawbacks: first, it requires that there be a closed outer conductor, which is not physical in many important cases. Second, as in the previous method, using elements which fill the entire cross-section increases the computation time unnecessarily, since only the value of the current and its normal derivative at the surface of the wire are needed to calculate the resistance.

A new method for analyzing frequency-dependent transmission line systems with nonlinear terminations is presented. The generalized scattering matrix formulation is used as the foundation for the time domain iteration scheme. Compared to the admittance matrix approach proposed in a previous paper, it has the advantage of shorter impulse response which leads to smaller computer memory requirement and faster computation time. Examples of a microstrip line loaded with nonlinear elements are given to illustrate the efficiency of this method.

As the speeds of integrated circuits increase, the effect of interconnection lines becomes more and more important. Traditional lumped element circuit model must be supplemented by the transmission line model in order to account for propagation delays, dispersion and losses. This has created needs for new numerical procedures that can be easily incorporated into current CAD tools. To make matters more complicated, the interconnection lines are terminated with not only linear resistors but also nonlinear semiconductor devices, such as diodes and transistors.

Several techniques are now commonly used to deal with nonlinear circuit problems, for example, the direct time domain approaches, and the semi-frequency-domain approaches, such as the harmonic balance technique. The semi-frequency-domain approaches are useful for microwave and millimeter wave integrated circuits but become impractical for digital integrated circuits because of the latter's wide band nature. On the other hand, frequency-dependent parameters often make it awkward to apply the direct time domain approach to the interconnection line systems.

We propose a hybrid frequency-domain time-domain technique based on the generalized scattering matrix formulation. For an n line system, we define $2n$ scattering parameters according to the frequency-dependent characteristic impedances of individual lines ($Z_{0j} = \sqrt{L_{jj}(\omega)/C_{jj}(\omega)}$). The time-domain transfer matrix (impulse response) of this $2n$-port system is then obtained by the inverse Fourier Transform. Lastly, the nonlinear equations associated with terminal characteristics are incorporated and solved with iteration procedures such as the Newton-Ralphson method.

The key to efficient and stable solutions in this problem is shortening the duration of every transfer matrix element. With the generalized scattering parameters approach, we are able to achieve that yet eliminating the need for artificial matching networks adopted by a previous work. Furthermore, the use of individual characteristic impedances in the definition of scattering parameters enables us to generalize this method to coupled lines with distinct properties while keeping the duration of transfer matrix elements short. This cannot be realized if traditional scattering parameters are used. We shall illustrate the elegance and efficiency of our approach for a dispersive microstrip line with different nonlinear loads and excited with narrow Gaussian pulses. The elements of transfer matrix are found out to be either zero or single retarded delta-impulse accompanying a small spike with very narrow spread. Typical computation time for a 1000 time-step iteration ranges from 4 to 27 seconds on a VAXStation 3500. The effects of line dispersion and load nonlinearity will be clearly delineated in the presentation.

The transient propagation characteristics of VLSI interconnects with discrete capacitive loads at various locations is analyzed based on a hybrid transmission lines-lumped element circuit model. Exact expressions of the Laplace transform of unit step responses are first obtained through the ABCD matrix formulation. We then apply the equivalent dominant pole approximation to the transfer function with the propagation delays factored out. The approximated transfer function can be inverted in closed form and quickly evaluated. These results provide efficient ways of finding approximately the effects on delays and rise time brought by VLSI off-chip interconnects.

Because of the dramatic increase in device densities on microelectronic chips, the propagation delay for off-chip interconnects has become the limiting factor to the speed of VLSI packages. Typical scales of these interconnects will be comparable or larger to the characteristic wavelength of high frequency components of the signal. Therefore, to calculate the delays caused by these interconnects properly, a hybrid circuit model containing transmission line sections as well as lumped elements must be used in place of the all-lumped element one. Most circuit simulation packages are nevertheless based on the latter and have to resort to subsection approximation when dealing with transmission lines. This scheme will undoubtedly lead to lengthy computation, which is not desirable when a quick, heuristic estimate of bounds are needed for the initial phase of the design cycle.

Two approaches have been developed for obtaining the approximate transient response without lengthy simulation. The first kind of solution techniques emphasize the calculation of bounds to voltage responses from the differential equations either by direct integration or by using the optimal control theory. On the other hand, the second kind of techniques analyze the properties of Laplace transform domain solution. Thus far, their applications are limited to all lumped-element and distributed RC networks, which can only take care of on-chip interconnects. We shall take the second approach by incorporating transmission line elements for off-chip delay estimation.

Our configuration includes a series of transmission line sections with arbitrary discrete capacitances and resistances loaded at junctions. The ABCD matrix formulation is used to obtain the Laplace transform of the unit step response. We express the latter in the form of $\exp(-sT)/Q(s)$, where $Q(s) = A_0(s) + A_1(s)\exp(s\tau_1) + A_2(s)\exp(s\tau_2) + \cdots$ with all $\{A_i(s)\}$ being rational functions in s. The factor $\{\exp(-sT)\}$ is identified with direct transmission delay over the total length of the line. For the rest part $(1/Q(s))$, we proceed to apply the equivalent dominant pole approximation technique[7]. Either a single negative real pole or second-order complex conjugate pair will be chosen for approximation depending upon the property of lumped loads at junctions as well as the source impedances. A phase-correction factor $\exp(-sT_m)$ is introduced to make up for the discrepancies caused by our low-order approximation. The first-order and second order approximations enable us to obtain closed-form solution to the transient response. Comparison of the approximated responses with those obtained from brute-force numerical Laplace inversion shows

very good match when the propagation delay of an average transmission line section is less than half the product of junction load capacitance and transmission line characteristic impedance. Yet we only have to spend a fraction of the time for computations. The accuracy of this method will be discussed in detail with some examples of lossless transmission line networks in which lumped capacitors are loaded at regular intervals.

The propagation properties of single and coupled inhomogeneous slab waveguides are analyzed. An integral equation formulation using the dyadic Green's function which covers both the TE and TM modes is proposed. The dispersion relations are obtained by applying the Galerkin's method to solve the integral equation. The coupling between two symmetrical inhomogeneous slab waveguides is also investigated. This method is shown to be applicable to arbitrary dielectric constant profiles.

The guidance and leakage properties of single and coupled dielectric strip waveguides are analyzed using the dyadic Green's function and integral equation formulation. Galerkin's method is used to solve the integral equation for the dispersion relation. The effects of the geometrical and the electrical parameters on the dispersion relation are investigated. A method to predict the occurrence of leakage is proposed. The properties of the even and the odd leaky modes are also investigated. Results are compared with previous analysis and shown to be in good agreement.

A spectral domain dyadic Green's function for multilayered uniaxially anisotropic media containing three-dimensional sources is derived. Tractable forms are shown to be easily deduced from the physical picture of the waves radiated by the primary sources and the multiple reflections from the stratified medium. The formulation decomposes the dyadic Green's function into TE and TM waves. The dyadic Green's function in the source region is properly represented by extracting the delta function singularity. A simple proceedure to obtain the fields in any arbitrary layer is described. Recursion relations for appropriately defined reflection and transmission coefficients are presented. Forms suitable for transmission line applications in multilayered media are derived.

Full modal analysis is used to study the dispersion characteristics of microstrip lines periodically loaded with crossing strips in a stratified uniaxially anisotropic medium. Dyadic Green's functions in the spectral domain for the multilayered medium in conjunction with the vector Fourier transform (VFT) are used to formulate a coupled set of vector integral equations for the current distribution on the signal line and the crossing strips. Galerkin's procedure is applied to derive the eigenvalue equation for the propagation constant. The effect of anisotropy for both open and shielded structures on the stopband properties is investigated.

A direct three dimensional finite difference time domain (FDTD) method is applied to the full-wave analysis of various microstrip structures. The method is shown to be an efficient tool for modelling complicated microstrip circuit components as well as microstrip antennas. From the time domain results, the input impedance of a line-fed rectangular patch antenna and the frequency dependent scattering parameters of a low pass filter and a branch line coupler are calculated. These circuits are fabricated and the measurements are compared with the FDTD results and shown to be in good agreement.

A rigorous dyadic Green's function formulation in the spectral domain is used to study the dispersion characteristics of signal strip lines in the presence of metallic crossing strips. A set of coupled vector integral equations for the current distribution on the conductors is derived. Galerkin's method is then applied to derive the matrix eigenvalue equation for the propagation constant. The dispersion properties of the signal lines are studied for both cases of finite and infinite length crossing strips. The effects of the structure dimensions on the passband and stopband characteristics are investigated. For crossing strips of finite length, the stopband is mainly affected by the period, the crossing strip length, and the separation between the signal and the crossing strips. For crossing strips of infinite length carrying travelling waves, attenuation along the signal line exists over the whole frequency range of operation.

PUBLICATIONS SUPPORTED BY ONR CONTRACT N00014-89-J-1019 SINCE 1988

A Macroscopic model of nonlinear constitutive relations in superconductors (J. Xia, J. A. Kong, and R. T. Shin), accepted for publication on the *IEEE Transactions on Microwave Theory and Techniques*, 1992.

Electromagnetic profile reconstruction using the Riccati equation approach (J. Xia and J. A. Kong), IEEE APS International Symposium, Chicago, Illinois, 18-25, July 1992.

Electromagnetic inverse scattering in remote sensing (J. Xia and J. A. Kong), Optical Society of America Topical Meeting on Signal Recovery and Synthesis, New Orleans, Louisiana, April 14–15, 1992.

Input impedance of a probe-fed stacked circular microstrip antenna (A. N. Tulintseff, S. M. Ali, and J. A. Kong), *IEEE Transactions on Antennas and Propagation,* Vol. 39, No. 3, 381-390, March 1991.

Analysis of diffraction from chiral gratings (S. H. Yueh and J. A. Kong), *Journal of Electromagnetic Waves and Applications,* Vol. 5, No. 7, 701-714, 1991.

Dyadic Green's functions in a planar stratified, arbitrarily magnetized linear plasma (T. M. Habashy, S. M. Ali, J. A. Kong, and M. D. Grossi), *Radio Science,* Vol. 26, No. 3, 701–716, May–June, 1991.

Current distribution, resistance, and inductance for superconducting strip transmission lines (D. M. Sheen, S. M. Ali, D. E. Oates, R. S. Withers, and J. A. Kong), *IEEE Transactions on Applied Superconductivity,* Vol. 1, No. 2, 108–115, June, 1991.

Integral equation solution to the guidance and leakage properties of coupled dielectric strip waveguides (J. F. Kiang, S. M. Ali, and J. A. Kong), *IEEE Transactions on Microwave Theory and Techniques,* Vol. 38, No. 2, 193–203, February 1990.

Application of the three dimensional finite difference time-domain method to the analysis of planar microstrip circuits (D. M. Sheen, S. M. Ali, M. D. Abouzahra, and J. A. Kong), *IEEE Transactions on Microwave Theory and Techniques*, Vol. 38, No. 7, 849–857, July 1990.

The propagation characteristics of signal lines with crossing strips in multilayered anisotropic media (C. W. Lam, S. M. Ali, and J. A. Kong), *Journal of Electromagnetic Waves and Applications,* Vol. 4, No. 10, 1005–1021, 1990.

Resonant frequencies of stacked circular microstrip antennas (A. N. Tulintseff, S. M. Ali, and J. A. Kong), *IEEE AP-S International Symposium and URSI Radio Science Meeting,* San Jose, California, June 26–30, 1989.

Probe excitation of a center-fed circular microstrip antenna employing a stratified medium formulation (S. M. Ali, T. M. Habashy, and J. A. Kong), *IEEE AP-S International Symposium and URSI Radio Science Meeting,* San Jose, California, June 26–30, 1989.

Probe excitation of a center-fed circular microstrip antenna employing the Weber Transform (T. M. Habashy, S. M. Ali, and J. A. Kong), *IEEE AP-S International Symposium and URSI Radio Science Meeting,* San Jose, California, June 26–30, 1989.

Input impedance and radiation fields of a probe-fed stacked circular microstrip antenna, (A. N. Tulintseff, S. M. Ali, and J. A. Kong), *Progress in Electromagnetics Research Symposium,* 508-509 Boston, Massachusetts, July 25–26, 1989.

Analysis of microstrip discontinuities on anisotropic substrates, (J. Xia, S. M. Ali, and J. A. Kong), *Progress in Electromagnetics Research Symposium,* 502-503, Boston, Massachusetts, July 25–26, 1989.

Analysis of dielectric strip waveguides using integral equation formulation, (J. F. Kiang, S. M. Ali, and J. A. Kong), *Progress in Electromagnetics Research Symposium,* 109-110, Boston, Massachusetts, July 25–26, 1989.

Input impedance of a circular microstrip antenna fed by an eccentric probe, (S. M. Ali, T. M. Habashy, and J. A. Kong), *Progress in Electromagnetics Research Symposium,* Boston, Massachusetts, 506-507, July 25–26, 1989.

Finite difference time domain techniques for two dimensional triangular grids, (C. F. Lee, R. T. Shin, J. A. Kong, and B. J. McCartin), *Progress in Electromagnetics Research Symposium,* 189-190, Boston, Massachusetts, July 25–26, 1989.

Absorbing boundary conditions on circular and elliptic boundaries, (C. F. Lee, R. T. Shin, J. A. Kong, and B. J. McCartin), *Progress in Electromagnetics Research Symposium,* 317-318, Boston, Massachusetts, July 25–26, 1989.

A new finite-difference time-domain grid model for microstrip problems in anisotropic media, (C. W. Lam, S. M. Ali, and J. A. Kong), *Progress in Electromagnetics Research Symposium,* 305-306, Boston, Massachusetts, July 25–26, 1989.

Analysis of multiport rectangular microstrip structures using a three dimensional finite difference time domain technique, (D. M. Sheen, S. M. Ali, M. D. Abouzahra, and J. A. Kong), *Progress in Electromagnetics Research Symposium,* 504-505, Boston, Massachusetts, July 25–26, 1989.

The frequency-dependent resistance of conductors with arbitrary cross-section, (M. J. Tsuk and J. A. Kong), *Progress in Electromagnetics Research Symposium,* 251-252, Boston, Massachusetts, July 25–26, 1989.

Transient analysis of frequency-dependent transmission lines with nonlinear terminations, (Q. Gu, Y. E. Yang and J. A. Kong), *Progress in Electromagnetics Research Symposium,* 239-240, Boston, Massachusetts, July 25–26, 1989.

Transient analysis of capacitively loaded VLSI off-chip interconnections, (Y. E. Yang and J. A. Kong), *Progress in Electromagnetics Research Symposium,* 241-242, Boston, Massachusetts, July 25–26, 1989.

Inversion of permittivity and conductivity profiles employing transverse-magnetic polarized monochromatic data (T. M. Habashy, M. Moldoveanu, and J. A. Kong), *SPIE's 1990 International Symposium on Optical and Optoelectronic Applied Science and Engineering,* San Diego, California, July 8–13, 1990.

Electro-magnetic calculation of soft X-ray diffraction from nanometer-scale gold structures (M. L. Schattenburg, K. Li, R. T. Shin, J. A. Kong, and H. I. Smith), submitted to *The 35th International Symposium on Electron, Ion, and Photon Beams,* Seattle, Washington, May 28–31, 1991.

Electromagnetic calculation of soft x-ray diffraction from 01.μm-scale gold structures (M. L. Schatenburg, K. Li, R. T. Shin, J. A. Kong, D. B. Olster, and H. I. Smith), *Journal of Vacuum Science and Technology* as part of the proceedings of *The 35th International Symposium on Electron, Ion, and Photon Beams,* (paper E84), Seattle, Washington, May 28–31, 1991.

A Macroscopic Model of Nonlinear Constitutive Relations in Superconductors

Jake Jiqing Xia

Jin Au Kong

Robert T. Shin

Department of Electrical Engineering and Computer Science

and Research Laboratory of Electronics

Massachusetts Institute of Technology

Cambridge, MA 02139

Abstract

A macroscopic model is proposed to explain nonlinear electromagnetic phenomena in superconductors. Nonlinear constitutive relations for electromagnetic problems are derived by modifying the linear London's equations. The superelectron number density n_s is a function of the applied current density J. The critical current density J_c is derived classically from a critical energy E_c. For temperature $T \neq 0$, the concept of critical current J_c does not imply an abrupt transition of the whole sample from a superconducting state to a normal state when $J > J_c$. A rather smooth variation of $n_s(J)$ is shown instead. The relation, $n_s(J)$, is derived from the Maxwellian distribution of electron velocities at a certain temperature T and a certain macroscopic current density J. Agreement has also been found between this $n_s(J,T)$ model and the temperature dependence of n_s in the two-fluid model. The nonlinear conductivities $\sigma_s(J)$ and $\sigma_n(J)$ are obtained from the London's equation and the $n_s(J)$ function. Nonlinear resistance $R(I)$, kinetic inductance $L_k(I)$ and surface impedance $Z_s(I)$ in thin wire, slab, and strip geometries of supercon-

ductors are calculated. A general scheme of solving nonlinear electromagnetic problems in superconductors is proposed. A good agreement between the theory and experiments has been found.

I. Introduction

Superconductors have great potential applications in many fields. For example, in microwave integrated circuits, high-Q resonators and microstrips can be made of superconductors for lower losses. The discovery of high-Tc superconductors has also made a big impact on superconductor modeling. The problem of modeling nonlinear electromagnetic properties of a superconductor is of practical importance. For example, in application of superconductors to high-Q resonators, fields and currents are very large at resonance. Nonlinear effects are inevitable.

In this paper, we use the macroscopic (classical) theory to model the nonlinear superconductivity. The constitutive relations which relate electric field $\overline{E}$ and magnetic field $\overline{B}$ to superconducting current density $\overline{J}_s$ will be derived. The theory is based on the two London equations and the two-fluid model. The new problem at hand is to incorporate the nonlinear effects into the constitutive relations. Application of the constitutive relations will provide new methods for studying nonlinear effects in superconductors.

There are different types of nonlinearity in superconductors. One type of nonlinearity is displayed in polycrystalline superconductors where granular currents are involved [1,2]. The granular nonlinearity occurs when the current I is above I_c (here I_c is the threshold current of the grain junctions). It is similar to a p-n junction's exponential I-V relation. It is also found in type II superconductors that the vortex motion in the mixing state (between the superconducting and the normal states) can cause a nonlinear $V - I$ relation when current density J is slightly greater than a critical current density J_c [3, p.331] [4, p.373]. The granular or vortex nonlinearity will not be discussed further in this paper.

Another type of nonlinearity is intrinsic for all superconductors. This is due to the de-

pendence of the superelectron number density n_s on the applied current density J. This nonlinearity is more general. There have been few papers in literature directly addressing this nonlinearity problem. In this paper we will focus on this intrinsic nonlinearity.

The purpose of this paper is to provide engineers a material-independent macroscopic model for nonlinearities in superconductors. The model will be based on macroscopic parameters. The model is intended to achieve the following: 1] to explain the nonlinear voltage-current ($V-I$) relations and the dependence of inductances on currents ($L-I$ relations). This requires the derivation of a complex conductivity $\tilde{\sigma}(J)$ model; 2] to explain the concept of critical current J_c with no abrupt transition in the sample's $V-I$ curve when J exceeds J_c; 3] to obtain the temperature dependence of $n_s(T)$ which agrees with what is assumed in the two-fluid model; 4] to derive a general scheme which can solve the nonlinear problem including the effects of geometry.

II. Critical Energy for a Single Electron, $E_c(T)$

The starting point of this model assumes that there is a critical value of energy, E_c, which separates the superconducting and normal states of a single electron. When an electron has an energy $E < E_c$, it is in the superconducting state, it is paired with another electron; when $E \geq E_c$, it is in the normal state. This critical value E_c is a function of temperature T. The higher T is, the lower E_c becomes. At $T = T_c$, the critical temperature, $E_c = 0$. This critical energy E_c reminds us the gap parameter Δ in the BCS microscopic theory. It may correspond to the de-pairing energy of a Cooper pair. But here the critical energy E_c is proposed as merely an assumption without justification. The origin of this E_c should be studied in microscopic theory. We will leave this problem and use E_c as a starting assumption.

We assume the temperature dependence of E_c as

$$E_c(T) = 3.52 k_B T_c (1 - \frac{T}{T_c})^{\alpha}, \qquad for \;\; 0 \leq T \leq T_c \tag{1}$$

where k_B is the Boltzmann constant, T_c is the critical temperature, and α is a free parameter which may depend on the type of material. $\alpha > 0$ is required.

For each electron, the energy consists of kinetic energy and potential energy,

$$E = E_k + E_p = \frac{1}{2} m v^2 + E_p \tag{2}$$

where m is the mass of an electron and v is its velocity. In quantum theory, v is the expectation value $< \psi | \hat{v} | \psi >$, where ψ is the wavefunction of the electron and $\hat{v}$ is the velocity operator. The electron energy E can be expressed as a function of temperature T, applied current density J, magnetic field H, and field frequency f.

$$E = E(T, J, f, H) \tag{3}$$

E_c is the origin for critical values of T_c, J_c, f_c and H_c. It is useful to determine the relations of these critical values to E_c.

III. Velocity Distribution for a Group of Electrons

First let's consider that the electrons have one-dimensional velocities, for example, in a thin (radius $a << \lambda$ the penetration depth) wire within which the current flows in only one direction. The electrons in the sample have different velocities due to thermal motion. The average velocity of all electrons is nonzero along the current direction. The current density J is a macroscopic quantity. At a certain point $\bar{r}$, J is related to the average velocity of the electrons in a small volume ΔV,

$$J = \frac{\sum_i^N q v_i}{\Delta V} \tag{4}$$

where N is the number of electrons in ΔV and q is the charge of an electron. Note that not every electron has the same velocity. The velocities v_i of the electrons obey a certain distribution. Here, for a particular example, we assume that the number of electrons, δN, which have the velocities between v and δv obeys the one-dimensional Maxwellian distribution. If we define

$$n(v) = \frac{\delta N}{\delta v \Delta V}, \tag{5}$$

then [10, p.80] [11, p.70]

$$n(v) = n_t \sqrt{\frac{m}{2\pi k_B T}} e^{-m(v-v_A)^2/2k_B T} \tag{6}$$

where v_A is the average velocity of the electrons, m is the mass of an electron, and n_t is a constant. The distribution is Gaussian. Figure 1 shows the $n(v)$ function. $n(v)$ is assumed to be a continuous distribution. The state of an electron will be determined from the velocity (energy) in this distribution $n(v)$.

The constant n_t can be determined from the normalization condition,

$$\int_{-\infty}^{+\infty} n(v)dv = n_0 \tag{7}$$

where n_0 is the total number density of electrons known at ΔV. It can be easily shown that

$$n_t = n_0. \tag{8}$$

We can relate the two macroscopic quantities, J and v_A. It can be shown that

$$J = \int_{-\infty}^{+\infty} qn(v)vdv = qn_0 v_A \tag{9}$$

at ΔV.

The T dependence of $n(v)$ shows that at $T = 0$,

$$n(v) = n_0 \delta(v), \tag{10}$$

a δ function [12, p.16]. When T becomes larger, the width $\sqrt{2k_BT/m}$ of the distribution is wider.

IV. $n_s(J)$ and Critical Current Density $J_c(T)$

Since the electrons have different velocities, therefore different energies at a certain applied current density J, the electrons will not all exceed the critical energy E_c at the same time. There is no macroscopic critical value J_c of the current density such that when $J > J_c$, number density of superelectrons $n_s = 0$. Only when $T = 0$ and $n(v)$ becomes $n_0\delta(v)$, $n_s(J)$ shows an abrupt drop to zero at a critical $J_c(T = 0)$: for $J < J_c(0)$, $n_s = n_0$; and for $J > J_c(0)$, $n_s = 0$. In experiments, since absolute $T = 0$K is not achievable, a completely sharp transition of n_s is not observed.

We can define a $J_c(T)$ which corresponds to the average velocity v_A and E_c. First, let's define a critical velocity v_c for a single electron corresponding to E_c. If the potential energy is included in the case of maximum kinetic energy, $\frac{1}{2}mv_c^2 = E_c$. Hence,

$$v_c = \sqrt{\frac{2E_c}{m}}. \tag{11}$$

Since $J = n_0qv_A$, we define

$$J_c(T) = qn_0v_c = qn_0\sqrt{\frac{2E_c(T)}{m}} \tag{12}$$

$$J_c(T) = qn_0\sqrt{\frac{7.04k_BT_c}{m}}(1 - \frac{T}{T_c})^{\alpha/2} \tag{13}$$

as the critical current density. This J_c is different from the Ginzburg-Landau's de-pairing current density. Here $J_c(T)$ is a quantity derived from the hypothetical critical energy E_c via the classical kinetic energy expression. The concept of this critical current density J_c is also different.

At $T \neq 0$, $n_s(J)$ is a smoothly varying function. The $J_c(T)$ has a different characteristics from $J_c(T=0)$. When $J > J_c(T)$, n_s does not go to zero. This smooth varying feature of the $I-V$ curve has been widely observed in experiments [5,6].

Since $v_A = J/qn_0$, the number density of superelectrons (here we count the single electron density rather than the pair density) $n_s(J)$ can be derived from the Maxwellian distribution. The superelectrons are those whose energy are lower than E_c.

$$n_s(J) = \int_{-v_c}^{v_c} n(v)dv = \int_{-v_c(T)}^{v_c(T)} n_0 \sqrt{\frac{m}{2\pi k_B T}} e^{-m(v-J/qn_0)^2/2k_BT} dv. \qquad (14)$$

In general, this integral can only be evaluated numerically. A special case is at $T=0$, $n(v) = n_0\delta(v-v_A)$. Hence, $n_s(J) = n_0$ if $v_A \leq v_c$ or $J \leq J_c(0)$; $n_s(J) = 0$ if $v_A > v_c$ or $J > J_c(0)$.

It is illustrated in Fig. 2 that when $v_A + \sqrt{2k_BT/m} < v_c$, almost all electrons are superelectrons, hence $n_s \approx n_0$; when $v_A - \sqrt{2k_BT/m} > v_c$, almost all electrons are normal electrons, hence $n_s \approx 0$. At $T = T_c$, $v_c = 0$, hence $n_s = 0$ for all J's. $n_s(J)$ is plotted in Fig. 3 for four different temperatures. Here J is normalized with the J_c at $T=0$. At $T=0$, $n_s = n_0$ for $J < J_c(0)$. This is what has been predicted by the two-fluid model.

The dependence of n_s on J has also been studied in the Ginzburg-Landau (GL) theory [4,7]. Figure 4 shows the $n_s(J)/n_s(J=0)$ function derived from the GL theory [4] with comparison to our model. In our model, n_s decreases smoothly to zero. The GL theory predicts that there is a critical J_c at all temperatures. When $J > J_c(T)$, $n_s = 0$, or n_s becomes an imaginary value. This $n_s(J)$ function was derived from minimizing the Gibbs free energy g_s. When minimizing g_s with respect to the order parameter ψ ($n_s = \psi\psi^*$), only a first few terms were taken in expanding g_s in terms of power series of ψ.

The GL theory is similar to the macroscopic quantum model (MQM) [4] for homogeneous samples. In the theory, all electrons are described by a single macroscopic wavefunction Ψ. Therefore all electrons have the same velocity, same as v_A. The distribution $n(v)$ is taken as $n_0\delta(v - v_A)$. Hence it predicts an abrupt drop of n_s to zero when $J > J_c(T)$ for all temperature T's. This is not what has been observed in experiments. Smooth variation of $n_s(J)$ is found for all J values. If the wavefunction of each electron ψ_i is taken into account for a distribution $n(v_i)$, where $v_i = < \psi_i|\hat{v}|\psi_i >$, a modified formula can be derived from statistical physics.

The original GL theory is for T close to T_c. The temperature dependence of n_s assumed in the two-fluid model is that

$$n_s(T) = n_0[1 - (\frac{T}{T_c})^4]. \tag{15}$$

The $n_s(T)$ function is compared with our distribution model in Fig. 5. From eq. (14), for a fixed J, the $n_s(T)$ curve matches the two-fluid model for $\alpha = 3/2$.

V. Conductivities $\sigma_s(J)$ and $\sigma_n(J)$

To derive the constitutive relations of superconductors for electromagnetic fields, we will use the London's equations. The London's equations are derived from the fundamental Newtonian dynamics and the Meissner effect [4]. They can also be derived from quantum mechanics by introducing a canonical momentum [3,8]. If we do not consider the Lorentz force due to the magnetic field, the linear London's equations are valid [4] from the Drude model and the Newton's second law.

$$\frac{\partial \overline{J}_s}{\partial t} = \frac{\overline{E}}{\Lambda} \tag{16}$$

$$\nabla \times \overline{J}_s = -\frac{\overline{B}}{\Lambda} \tag{17}$$

where $\overline{E}$ and $\overline{B}$ are the total electric and magnetic fields respectively, $\overline{J}_s$ is the current density due to superelectrons, and $\Lambda = m_s/q_s^2 n_s$. The subscript s denotes that the quantity is of superelectrons. The nonlinearity will be included in $\Lambda(J) = \mu_0 \lambda^2$, and

$$\lambda(J) = \sqrt{\frac{m_s}{q_s^2 n_s(J)\mu_0}}. \tag{18}$$

Once $n_s(J)$ is known, $\lambda(J)$ can be derived. Hence, the nonlinear constitutive relations are obtained. Nonlinear effects come in Λ and n_s.

Substituting eq. (14) of $n_s(J)$ in λ, we derive the $\lambda(J)$ function, which is plotted in Fig. 6. The penetration depth goes to infinity when $J >> J_c(T)$. Conductivities $\sigma_s(J)$ and $\sigma_n(J)$ are derived from the London equations for time-harmonic ($e^{-i\omega t}$) fields

$$\sigma_s = \frac{i q_s^2 n_s}{\omega m_s} \tag{19}$$

and

$$\sigma_n = \frac{q^2 n_n \tau}{m(1 - i\omega\tau)} \tag{20}$$

where

$$n_s(J) = \int_{-v_c}^{v_c} n(v)dv = \int_{-v_c(T)}^{v_c(T)} n_0 \sqrt{\frac{m}{2\pi k_B T}} e^{-m(v - J/qn_0)^2/2k_B T} dv$$

and the number density of normal electrons $n_n(J) = n_0 - n_s(J)$ from conservation of charge. The above equations are the key results of this paper. The conductivities are plotted in Fig. 7a and 7b, where τ is the transport time or the mean scattering time of normal electrons. $\sigma_s(J)$ and $\sigma_n(J)$ reflect the current dependence of n_s and n_n respectively. These plots are for $T = 88$K very close to the critical temperature $T_c = 90$ K. The nonlinear behavior is easy to see. Total conductivity is a complex number

$$\tilde{\sigma}(J) = \sigma_n(J) + \sigma_s(J) \tag{21}$$

VI. Geometry Effect in Nonlinear Relations

1. Thin wire

For a thin wire superconductor with radius $a << \lambda$, the current density J can be assumed independent of the radius ρ. The thin wire is an ideal case since $a << \lambda$ is not practical. Usually $\tau \approx 10^{-12}$ sec, and $\omega < 10^9$ Hz, hence $\omega\tau << 1$ which is the quasi-static case. $\sigma_n \approx \frac{q^2 n_n \tau}{m}$. Here we can not assume $|\sigma_s| >> |\sigma_n|$ since we are studying the transition where n_s may become very small.

Resistance per unit length of the wire can be written as

$$R = \frac{|\sigma_n|}{[|\sigma_n|^2 + |\sigma_s|^2]\pi a^2}. \tag{22}$$

The kinetic inductance L_k per unit length of the wire can be written as

$$L_k = \frac{|\sigma_s|}{[|\sigma_n|^2 + |\sigma_s|^2]\omega\pi a^2}. \tag{23}$$

In this case, the internal and external inductances, L_{in} and L_{ex}, related to the energy stored in the magnetic field are independent of I, therefore are linear. Figure 8 show the calculated $R - I$ and $L_k - I$ curves from eqs. (22) and (23), where $\omega\tau = 10^{-3}$, $I = J\pi a^2$. The $R - J$ curve appears very nonlinear because $T = 88$K is very close to $T_c = 90$K. One interesting behavior in the $L_k - J$ curve is that a maximum L_s appears near J_c. This can be explained from eq. (23). At $J << J_c(T)$, $n_s >> n_n\omega\tau$, hence $L_k \approx 1/n_s$ is small. At $J >> J_c(T)$, $n_n\omega\tau >> n_s$, hence, $L_k \approx n_s/(n_n)^2$ is also small. When $n_n\omega\tau$ and n_s are comparable, a maximum of L_k may be achieved.

A special case is that at DC where $\omega = 0$. From eq. (19), $\sigma_s \to \infty$. From the first London equation, $\overline{E} = \frac{\partial \overline{J}_s \Lambda}{\partial t} = 0$. When $J >> J_c$, $n_s \to 0$, then it is possible for $\overline{E} \neq 0$. If J_s has a small time fluctuation, then $\frac{\partial}{\partial t}$ is not exactly zero, the above quasi-static discussion can be applied.

2. Slab

The above discussion has not taken into account the geometry of the superconductor. For finite dimension superconductors, for example, a slab in Fig. 9, the non-uniform distribution of current density $J_y(x)$ will cause the nonlinearity occur earlier in the $R-I$ and L_k-I curves. The internal and external inductances L_{in} and L_{ex} will also be nonlinear since $J_y(x)$ is determined by I,

$$I = \iint J_y ds = \int dz \int dx J_y(x) = \int dz \int dx \tilde{\sigma}(x) E(x) \tag{24}$$

where $E(x)$ is the electric field. For a uniform current density, $J_y(x) = J_A$, $J_A = I/\Delta z d$ where d is the thickness of the slab. For non-uniform $J_y(x)$, at the edge of the slab, J_y is bigger than J_A, $n_s(J)$ is smaller at the edge. Therefore, for the same magnitude of I, inhomogeneous $J_y(x)$ will exceed J_c at some x's even when J_A is less than J_c.

If a three-dimensional velocity distribution is considered for a current flow in the y direction,

$$n(v_x, v_y, v_z) = n_0 (\frac{m}{2\pi k_B T})^{\frac{3}{2}} e^{-m[v_x^2 + (v_y - v_A)^2 + v_z^2]/2k_B T} \tag{25}$$

$J_y = q n_0 v_A$ and

$$lim_{T \to 0} n(\overline{v}) = n_0 \delta(v_x) \delta(v_y - v_A) \delta(v_z) \tag{26}$$

$$n_s(J_y) = \int_{-v_c}^{v_c} dv_y \int_{-\sqrt{v_c^2 - v_y^2}}^{\sqrt{v_c^2 - v_y^2}} dv_x \int_{-\sqrt{v_c^2 - v_y^2 - v_x^2}}^{\sqrt{v_c^2 - v_y^2 - v_x^2}} n(\overline{v}) dv_z \tag{27}$$

with $v_A = J_y / q n_0$.

Under the quasi-static condition $\omega\tau << 1$, if a current I is applied along y direction in the slab, a magnetic field $H_z(x)$ will result from the applied current $J_y(x)$. Note that in the finite-width slab of a linear superconductor, even at $\omega = 0$, current $J_y(x)$ has a non-uniform distribution, due to the penetration depth λ. From the second London equation

(17) and $\nabla \times \overline{A} = \overline{B}$, $\nabla \times \overline{H} = \overline{J}$, under the London gauge, $\nabla \cdot \overline{A} = 0$ and

$$\overline{A} = -\Lambda \overline{J}_s, \tag{28}$$

$$\nabla^2[J_s \lambda^2(J)] = J_s + J_n = J \tag{29}$$

where $\overline{A}$ is the vector potential. In general, this equation can not be solved in a closed-form.

Let's first consider the solution of a linear superconductor for $n_s >> n_n \omega \tau$.

$$J_y(x) = \frac{I}{2\lambda} \frac{\cosh(x/\lambda)}{\sinh(d/2\lambda)} \quad for \ \ |x| \leq d/2 \tag{30}$$

and

$$H_z(x) = -\frac{I}{2} \frac{\sinh(x/\lambda)}{\sinh(d/2\lambda)} \quad for \ \ |x| \leq d/2. \tag{31}$$

An iterative scheme is to use the linear solution $J_y(x)$ in eq. (30) to calculate $n_s(J)$ in eq. (14) and $\lambda(x)$ in eq. (18). Then λ in eq. (30) is substituted by the obtained $\lambda(x)$ to calculate $J_y(x)$. Then eq. (14) is used to calculate $n_s[J_y(x)]$ again. This procedure is repeated until $J_y(x)$ converges. Figure 10 shows the results of $J(x)$ and $\sigma_s(x)$ obtained from the iterative method.

The impedance of the slab is defined as

$$Z = \frac{1}{\int_{-d/2}^{d/2} dx \tilde{\sigma}(x)} \tag{32}$$

and resistance $R = Re(Z)$ and $L_k = -Im(Z)/\omega$. Figure 11 shows the $R - I$, $L_k - I$ relations from final convergent $J_y(x)$.

For different thicknesses d, the nonlinear curves are different. We have found that for smaller d/λ, $R - I$ and $L_k - I$ relations are more nonlinear. This is understandable since J_y is bigger for smaller d at a given applied current I.

Surface impedance of a superconductor is defined as

$$Z_s = \sqrt{\frac{\mu_0}{\tilde{\epsilon}}} \tag{33}$$

where

$$\tilde{\epsilon} = \epsilon + \frac{i\tilde{\sigma}(J)}{\omega}. \tag{34}$$

Surface resistance is $R_s = Re(Z_s)$, and surface inductance is $L_s = -Im(Z_s)/\omega$. For $\omega\tau = 10^{-3}$, R_s and L_s are plotted in Fig. 12. The nonlinear region appears near J_c where the sample is partially superconducting. In the normal or superconducting states, the relations are linear. The L_s is different at normal region and superconducting region.

Experimental results [13] are also compared in Fig. 12c. As it shows, this model agrees with the trend of the experimental results. Since some parameters (α, τ, etc.) are material dependent, by adjusting these parameters, a better fit between the theory and measurements may be found. Surface impedance Z_s is a good description of superconductors since most of the current and field are confined within the penetration depth λ from the surface.

Another case is at very high frequencies and σ_n for $T > T_c$ is not very big (which is true for the ceramic high T_c superconductors) so that ϵ can not be neglected in eq. (34) for J_y near J_c. Since $\frac{\partial}{\partial t} \neq 0$ in the Maxwell's equations, a wave equation has to be considered. We will solve the guided wave case where the electric field E_y is decaying away outside the slab.

The wave equation for E is

$$\nabla^2 E + k_0^2 \tilde{\epsilon_r} E = 0 \tag{35}$$

where

$$\tilde{\epsilon_r} = 1 + \frac{i\sigma(\tilde{J})}{\omega\epsilon_0}. \tag{36}$$

If we replace E by $\tilde{\sigma} J_y$ in eq. (35), eq. (35) will look very similar to eq. (29). We can also use an iterative scheme to solve for the nonlinear $\tilde{\sigma}$ case. First we assume σ is independent of J, solve for $J_y(x)$. Second we calculate $\sigma(x) = \sigma[J_y(x)]$. Third we solve the wave equation for the inhomogeneous medium problem, get $J_y(x)$. These steps will be repeated until $J_y(x)$ and $\tilde{\sigma}(x)$ converge. This is a feed-back process, at the edge, J_y increases will cause n_s decreases, hence σ_s decreases, hence J_y decreases, until stabilized.

This procedure is similar to solving the coupled two differential equations in the GL theory. Where the equation for $\overline{A}$ is essentially the same as the wave equation (35) for E or J_y. The difference is the second equation for ψ, where $\psi(\overline{A})$ ($n_s(J)$) will be derived. We derived $n_s(J)$ from the Maxwellian distribution, while the GL theory derived from minimizing Gibbs free energy at equilibrium. A macroscopic wave function (order parameter) is used to describe all electrons in the GL theory, hence the distribution of velocity diversity is neglected.

3. Thin film strip

The slab geometry results can be used to study a microstrip geometry. If the dimension of z in Fig.9 is squeezed to $d << \lambda$, the current will still be uniform in the z direction. Therefore the same results can be applied.

This nonlinear study can also be applied to the magnetic field H dependence of R and L. Once the relation between the magnetic field H and the current J is determined, H_c and J_c are related. The above discussion can be directly applied.

Although the model is classical, the corresponding quantum statistical distribution can be used to derive the velocity (energy) distribution. Discrete distribution may be needed if the energy is quantized.

VII. Conclusion

A macroscopic model is established for nonlinear constitutive relations in superconductors. Maxwellian distribution of electron velocities is used to derive the dependence of superelectron density n_s on applied current density J. Complex $\bar{\sigma}(J)$ is obtained. The geometry of a superconductor will introduce non-uniform distribution of the current density J. Therefore nonlinearity will be enhanced at the surface of the device. By using this macroscopic model, a general scheme of solving for electromagnetic properties of superconductors has been proposed.

Acknowledgement

This work was supported in part by the US Office of Naval Research under contracts N00014-89-J-1019 and N00014-90-J-1002.

References

[1] P. England, et al., "Granular superconductivity in $R_1Ba_2Cu_3O_{7-\delta}$ thin films", Phy. Rev. B, Vol.38, No.10, pp. 7125–7128, Oct. 1988.

[2] M.A. Dubson, et al., "Non-Ohmic regime in the superconducting transition of Polycrystalline $Y_1Ba_2Cu_3O_x$", Phy. Rev. Lett., vol.60, No.11, pp.1061–1064, Mar. 1988.

[3] T. Van Duzer and C.W. Turner,"Principles of Superconductive Devices and Circuits", New York: Elsevier, 1981.

[4] T.P. Orlando and K.A. Delin, "Foundations of Applied Superconductivity", Addison-Wesley Publishing Company, 1991.

[5] D.H. Kim, et al., "Possible origins of resistive tails and critical currents in high-temperature superconductors," Phys. Rev. B., vol. 42, No. 10, pp.6249-6258, 1990.

[6] X. Yu and M. Sayer, "Temperature dependence of critical currents in YBaCuO ceramics," Phys. Rev. B., vol.44, No.5, 1991-I

[7] L. N. Shehata, "The wall energy and the critical current of an anisotropic high-temperature superconductor using modified Ginzburg-Landau Theory," J. Low Temperature Phys., vol.78, No.1/2, 1990.

[8] M. Tinkham, "Introduction to Superconductivity," McGraw-Hill Book Inc., 1975.

[9] K.K. Mei and G.C. Liang, "Electromagnetics of superconductors", IEEE Trans. MTT, vol.39, No.9, Sept., 1991.

[10] L.D. Landau and E.M. Lifshitz, "Statistical Physics", Addison-Wesley, 1969.

[11] G.H. Wannier, "Statistical Physics", John Wiley & Sons, 1966.

[12] C.M. Bender and S.A. Orszag, "Advanced Mathematical Methods for Scientists and Engineers," McGraw-Hill Book Com., 1978.

[13] Y. Kobayashi, T. Imai and H. Kayano, "Microwave measurements of temperature and current dependences of surface impedance for high-T_c superconductors," IEEE Trans. on Microwave Theory and Techniques, vol. 39, No.9, pp.1530-1538, Sept. 1991.

Figure Captions

Fig. 1. Maxwellian distribution of electron velocities.

Fig. 2. $n(v)$ functions for different average velocity v_A's.

Fig. 3. $n_s(J)/n_0$ at different temperatures. In this example, $\alpha = 3/2$, and $T_c = 90\text{K}$. $J_c(0)$ is from eq. (13).

Fig. 4. Comparison between the GL theory and this model for $n_s(J)/n_s(J=0)$ at $T = 88\text{K}$. Here $\alpha = 3/2$, $T_c = 90\text{K}$.

Fig. 5. Comparison between the two-fluid model and this model for $n_s(T)/n_0$ at $J = 0$. Here $T_c = 90\text{k}$.

Fig. 6. Penetration depth λ as a function of current density J at $T = 88\text{K}$. Here $\alpha = 3/2$, $T_c = 90\text{K}$.

Fig. 7. (a) super-conductivity σ_s as a function of J at $T = 88\text{K}$. Here $\alpha = 3/2$, $T_c = 90\text{K}$. (b) normal conductivity σ_n as a function of J at $T = 88\text{K}$. Here $\alpha = 3/2$, $T_c = 90\text{K}$.

Fig. 8. (a) Resistance of a thin wire R as a function of J at $T = 88\text{K}$. Here $\alpha = 3/2$, $T_c = 90\text{K}$. (b) Kinetic inductance L_k of a thin wire as a function of J at $T = 88\text{K}$. Here $\alpha = 3/2$, $T_c = 90\text{K}$.

Fig. 9. A superconducting slab with a thickness d.

Fig. 10. (a) Current density $J_y(x)$ distribution in a slab. (b) super-conductivity $\sigma_s(x)$ distribution in a slab. These are for $T = 80\text{K}$ and $\alpha = 3/2$, $T_c = 90\text{K}$, $d/\lambda(J=0) = 2$.

Fig. 11. For $d/\lambda(J=0) = 0.5, 1, 2$, (a) resistance of a slab, R, as a function of applied current intensity I at $T = 80\text{K}$; (b) kinetic inductance L_k of a slab as a function of

applied current intensity I at $T = 80$K. Here $\alpha = 3/2$, $T_c = 90$K.

Fig. 12. (a) Surface resistance R_s as a function of J at $T = 88$K and (b) surface inductance L_s as a function of J at $T = 88$K, Here $\alpha = 3/2$, $T_c = 90$K. (c) R_s as a function of surface current density K at $T = 77$k. The circles are the measured data from reference [14], The sample is a YBCO at $f = 10.4$GHz with $T_c = 92$K. The solid curve is the prediction from this model, where $\alpha = 3/2$, and $\omega\tau = 2.8X10^{-2}$. The surface current density is calculated from J with a thickness of $\lambda(J)$.

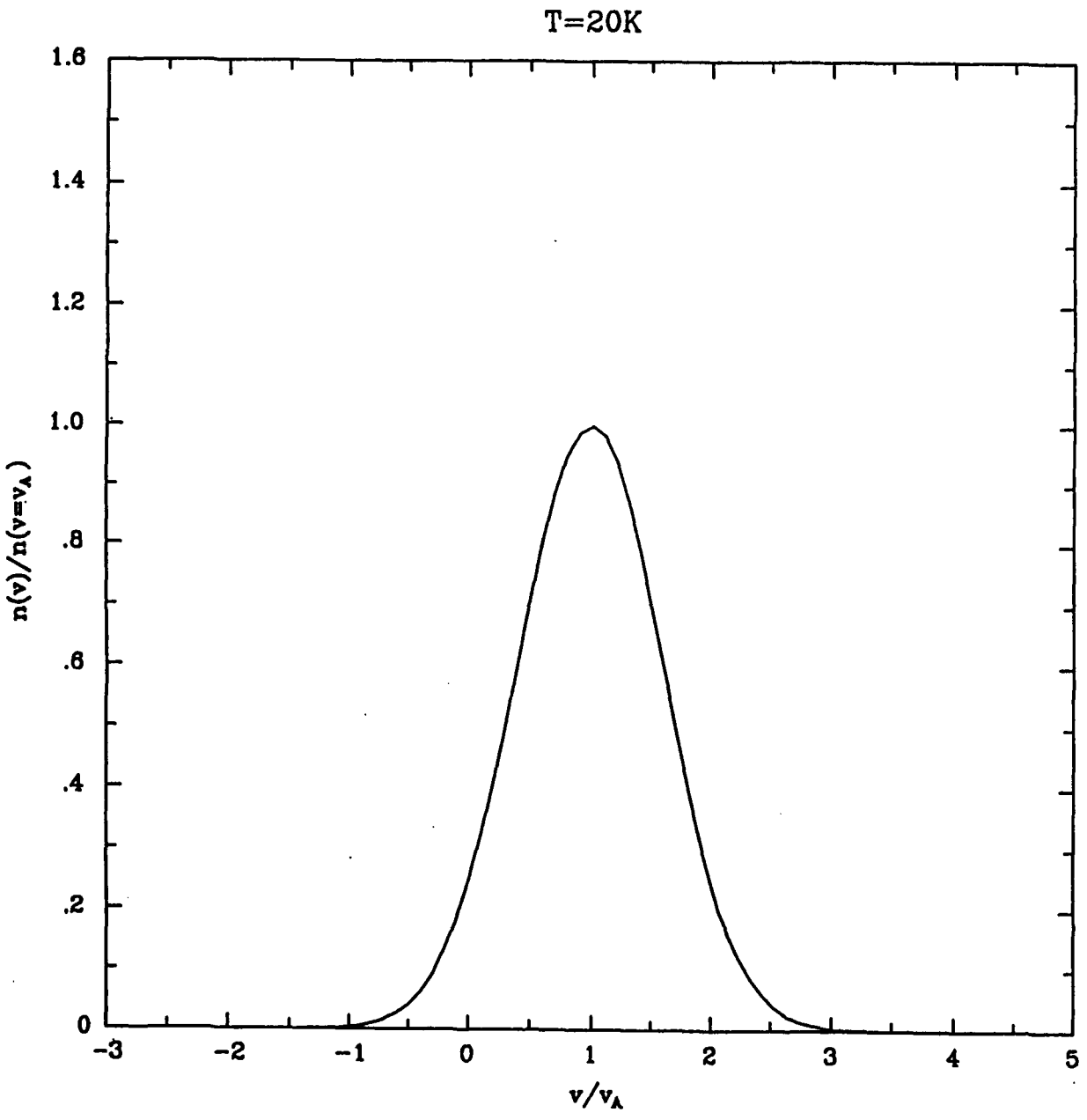

Fig. 1

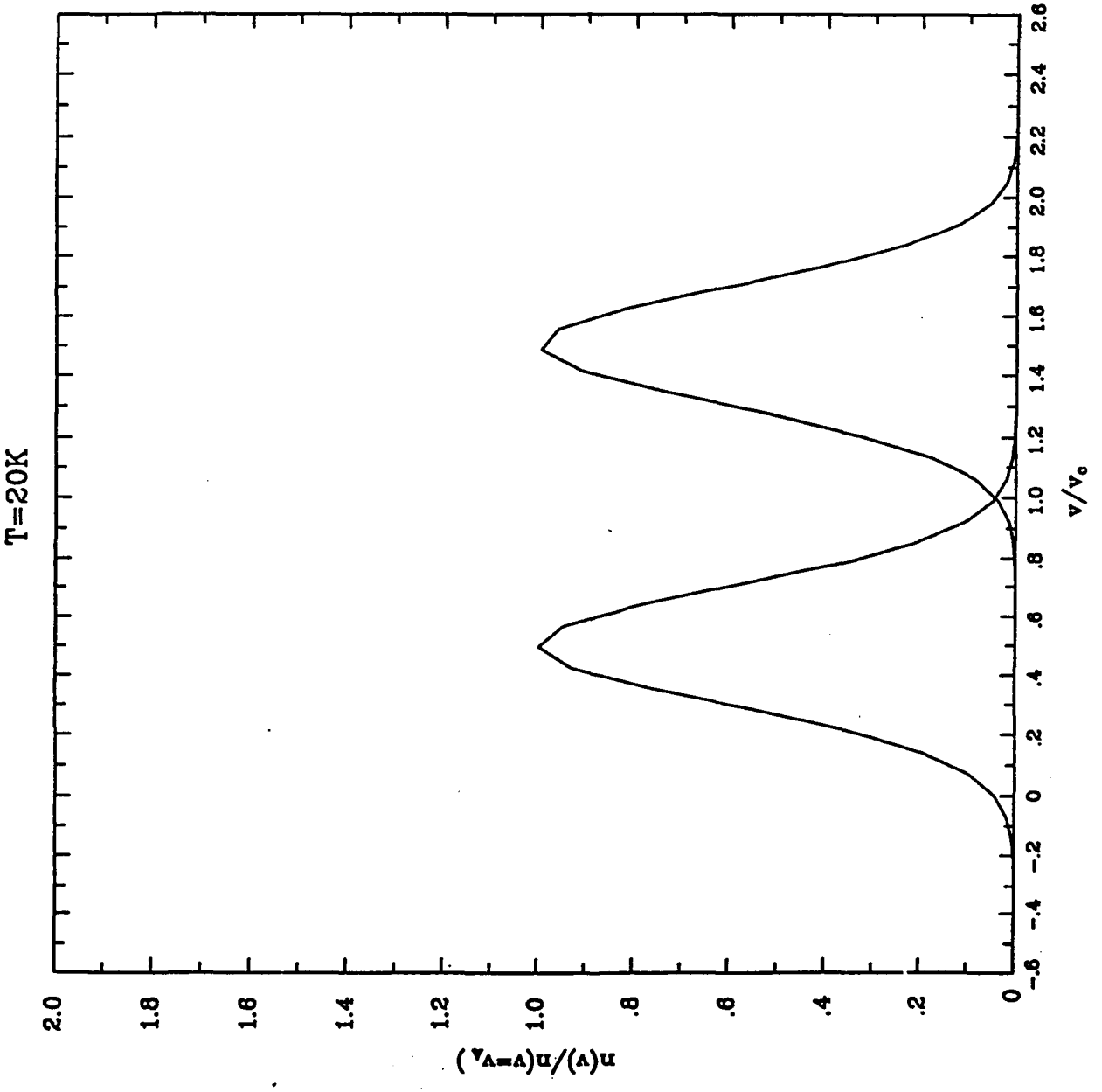
T=20K
n(v)/n(v=v_A)
v/v_o
2.0
1.8
1.6
1.4
1.2
1.0
.8
.6
.4
.2
0
-.6
-.4
-.2
0
.2
.4
.6
.8
1.0
1.2
1.4
1.6
1.8
2.0
2.2
2.4
2.6

Fig. 2

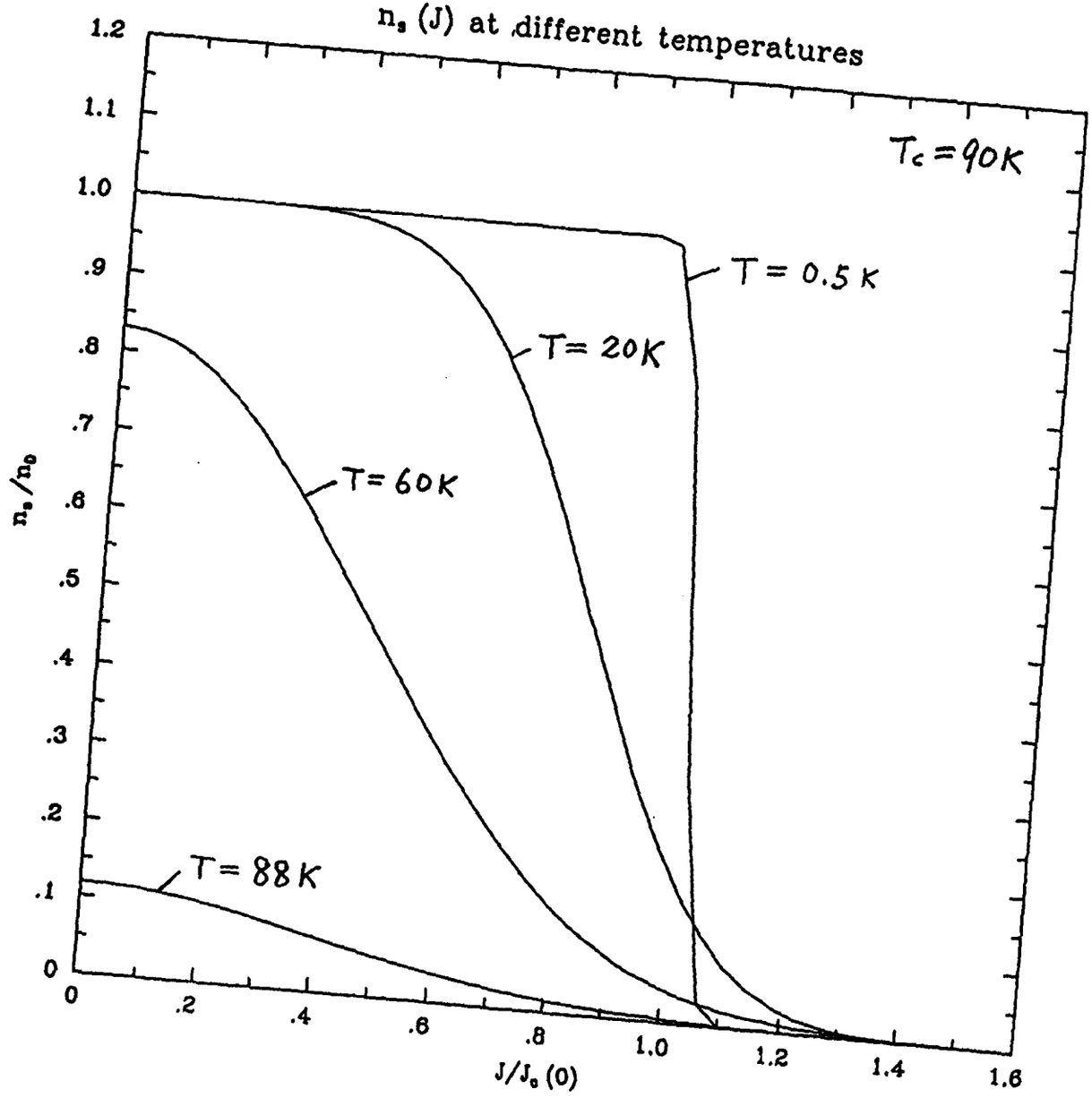
n_s (J) at different temperatures
$T_c = 90K$
T = 0.5 K
T= 20K
T= 60K
T= 88K
n_s/n_0
J/J_0 (0)
1.2
1.1
1.0
.9
.8
.7
.6
.5
.4
.3
.2
.1
0
0
.2
.4
.6
.8
1.0
1.2
1.4
1.6

Fig. 3

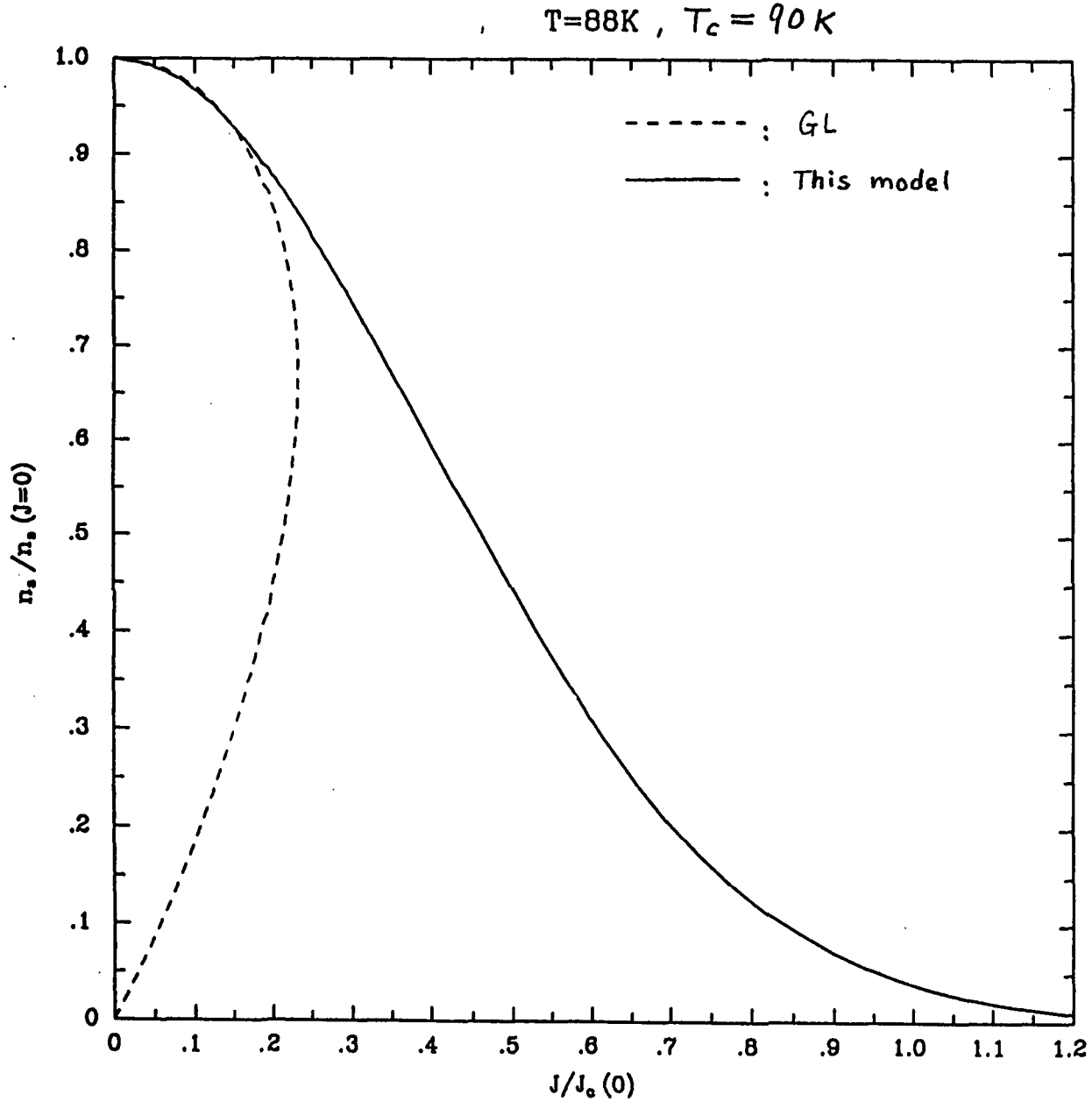
T=88K , $T_c = 90\,K$
------ : GL
——— : This model
$n_s/n_s\,(J=0)$
$J/J_c\,(0)$
1.0
.9
.8
.7
.6
.5
.4
.3
.2
.1
0
0
.1
.2
.3
.4
.5
.6
.7
.8
.9
1.0
1.1
1.2

Fig. 4

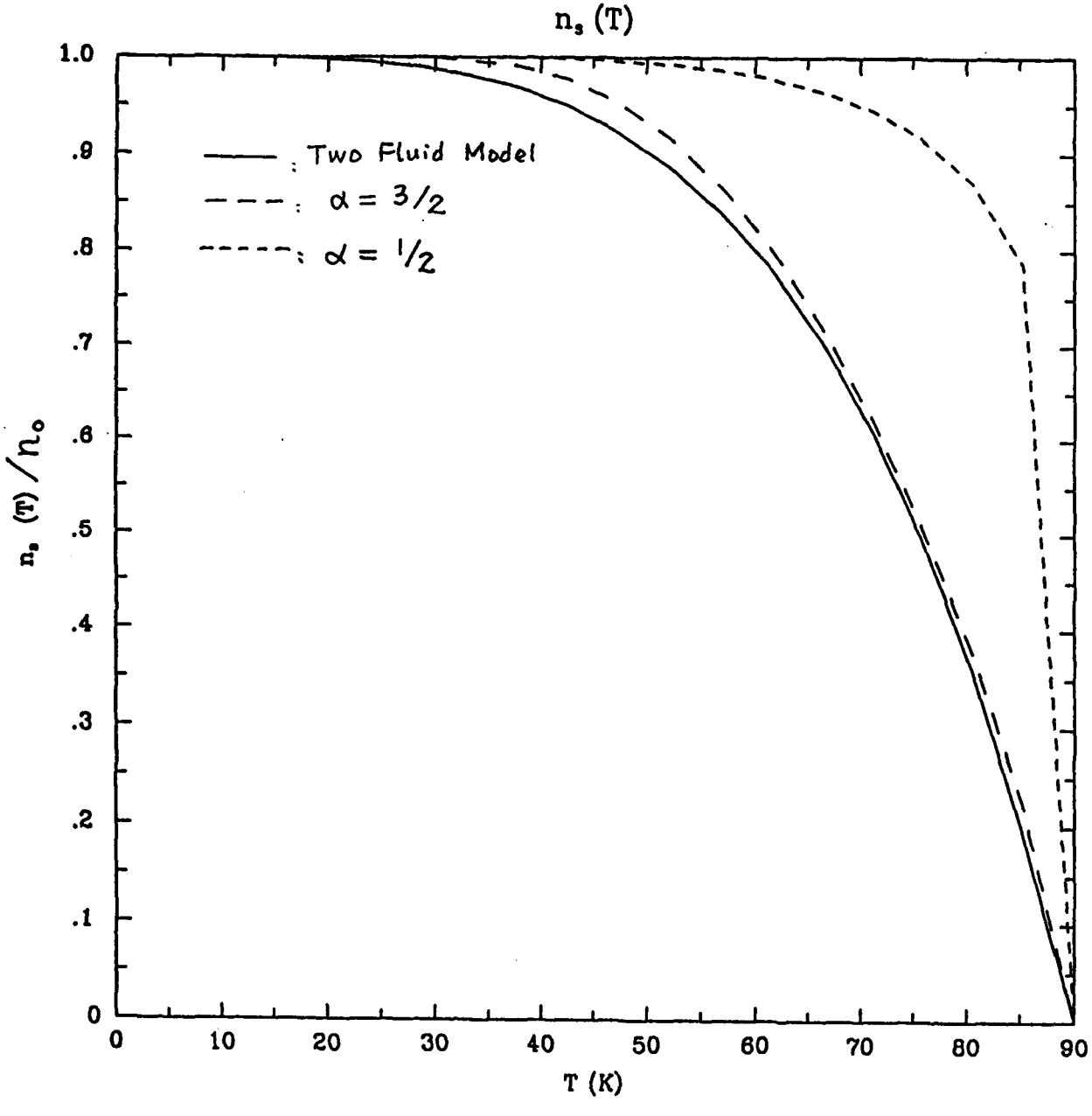
n_s (T)
1.0
.9
.8
.7
.6
.5
.4
.3
.2
.1
0
n_s (T) / n_o
Two Fluid Model
$\alpha = 3/2$
$\alpha = 1/2$
0
10
20
30
40
50
60
70
80
90
T (K)

Fig. 5

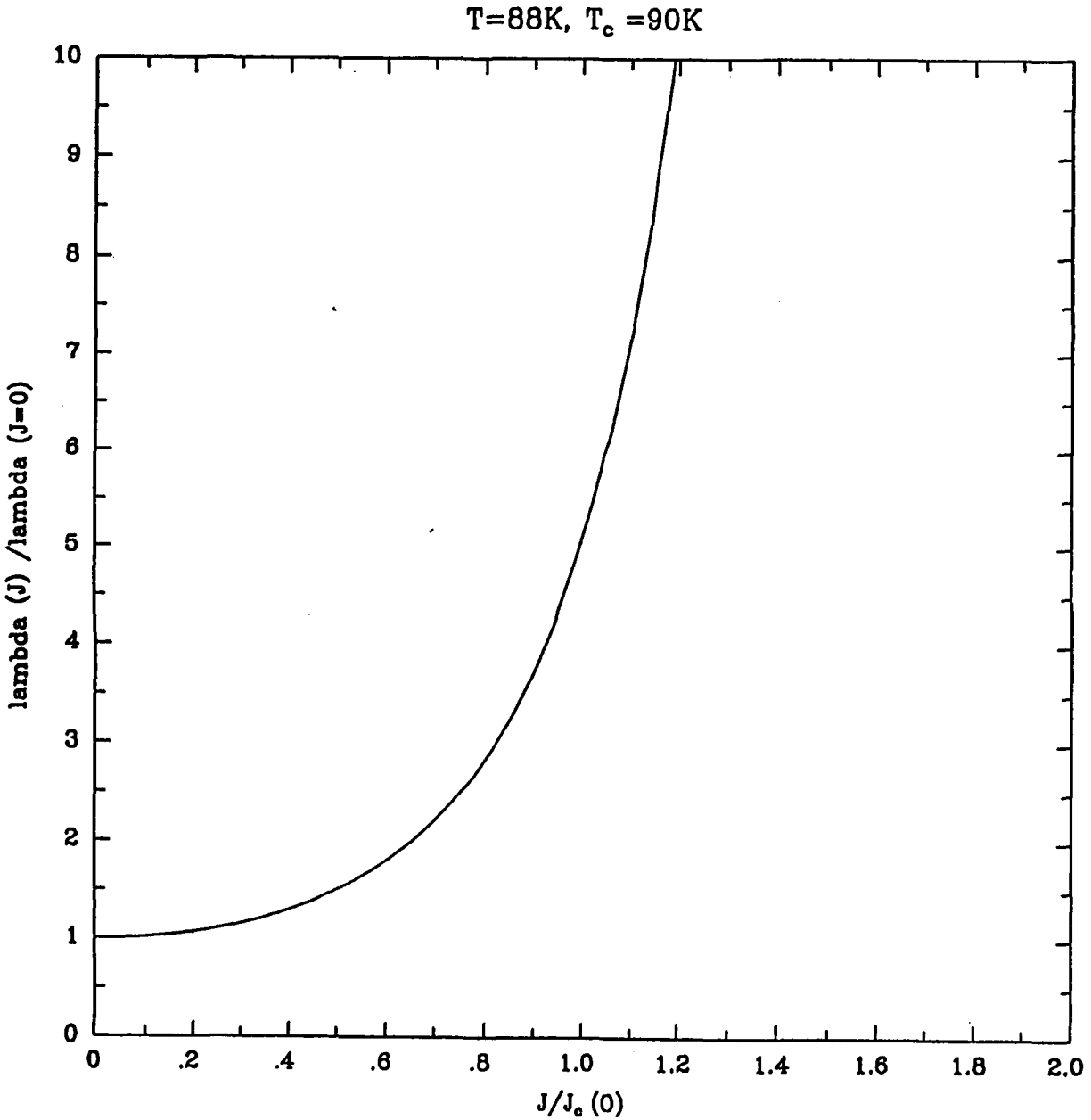
T=88K, T_c =90K
lambda (J) /lambda (J=0)
J/J_c (0)
0
.2
.4
.6
.8
1.0
1.2
1.4
1.6
1.8
2.0
1
2
3
4
5
6
7
8
9
10

Fig. 6

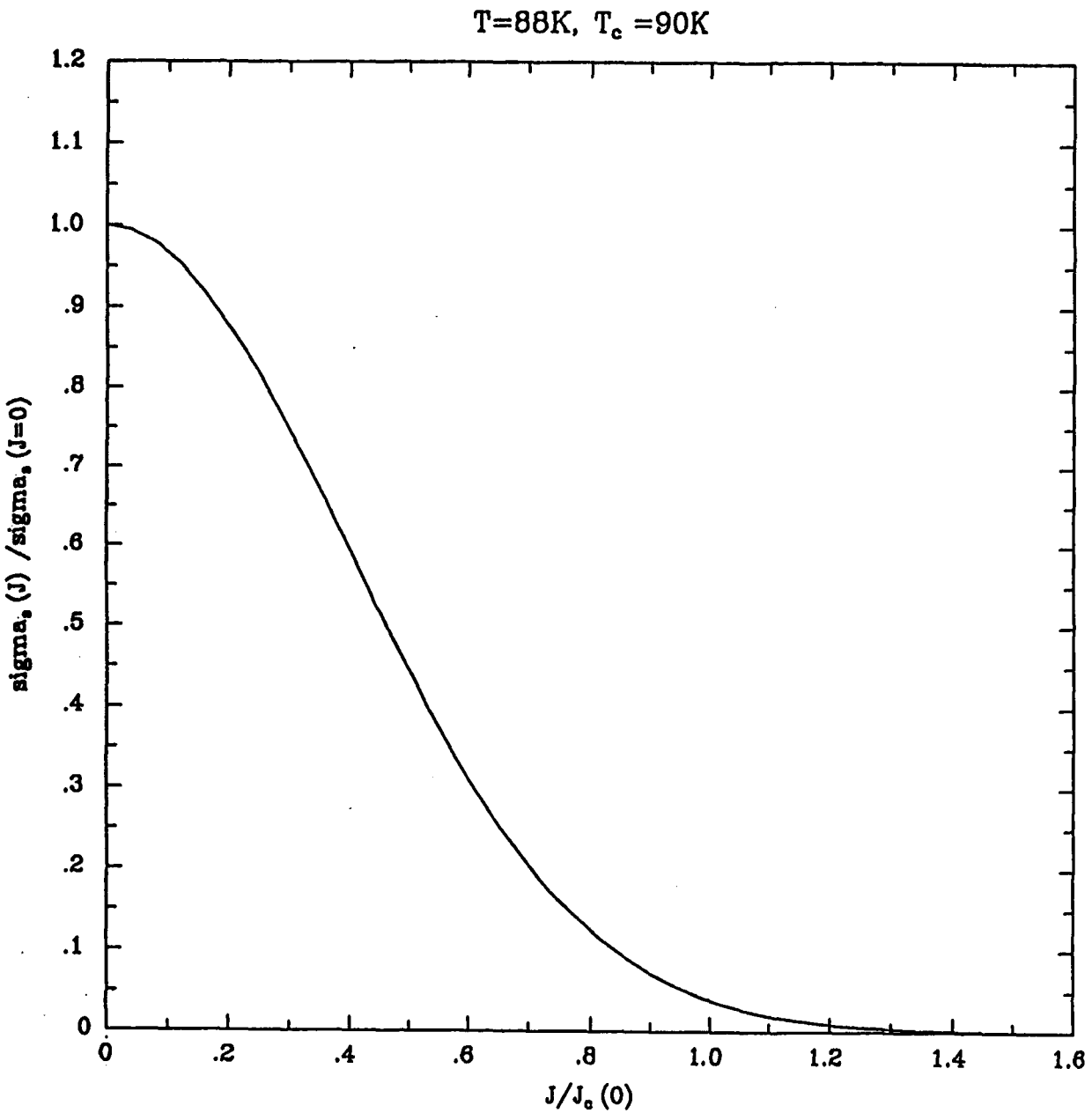
T=88K, T_c =90K
1.2
1.1
1.0
.9
.8
.7
.6
.5
.4
.3
.2
.1
0
sigma$_s$ (J) /sigma$_s$ (J=0)
0
.2
.4
.6
.8
1.0
1.2
1.4
1.6
J/J_c (0)

Fig. 7a

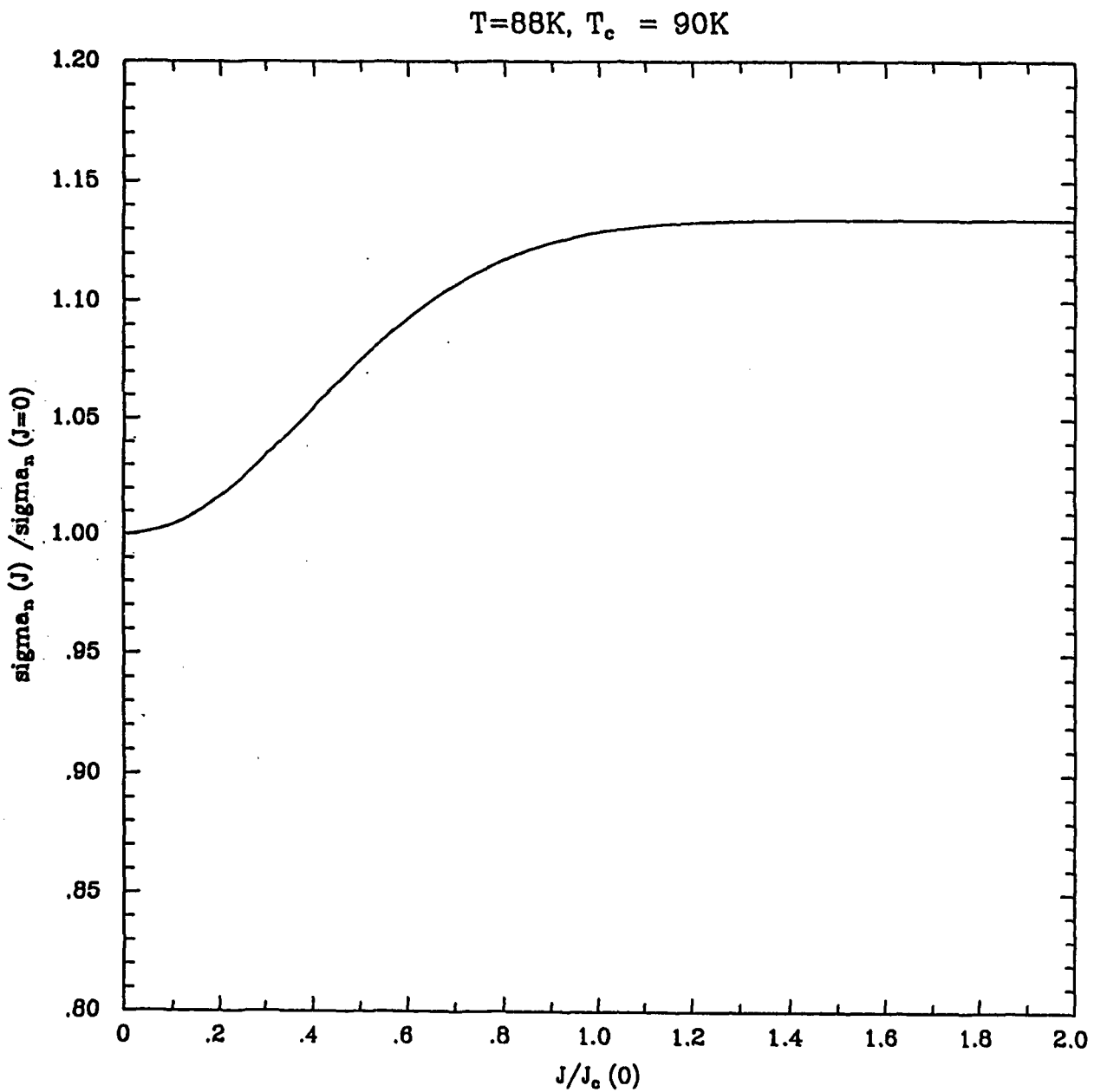
T=88K, T_c = 90K
1.20
1.15
1.10
1.05
1.00
.95
.90
.85
.80
$sigma_n$ (J) /$sigma_n$ (J=0)
0
.2
.4
.6
.8
1.0
1.2
1.4
1.6
1.8
2.0
J/J_c (0)

Fig. 7b

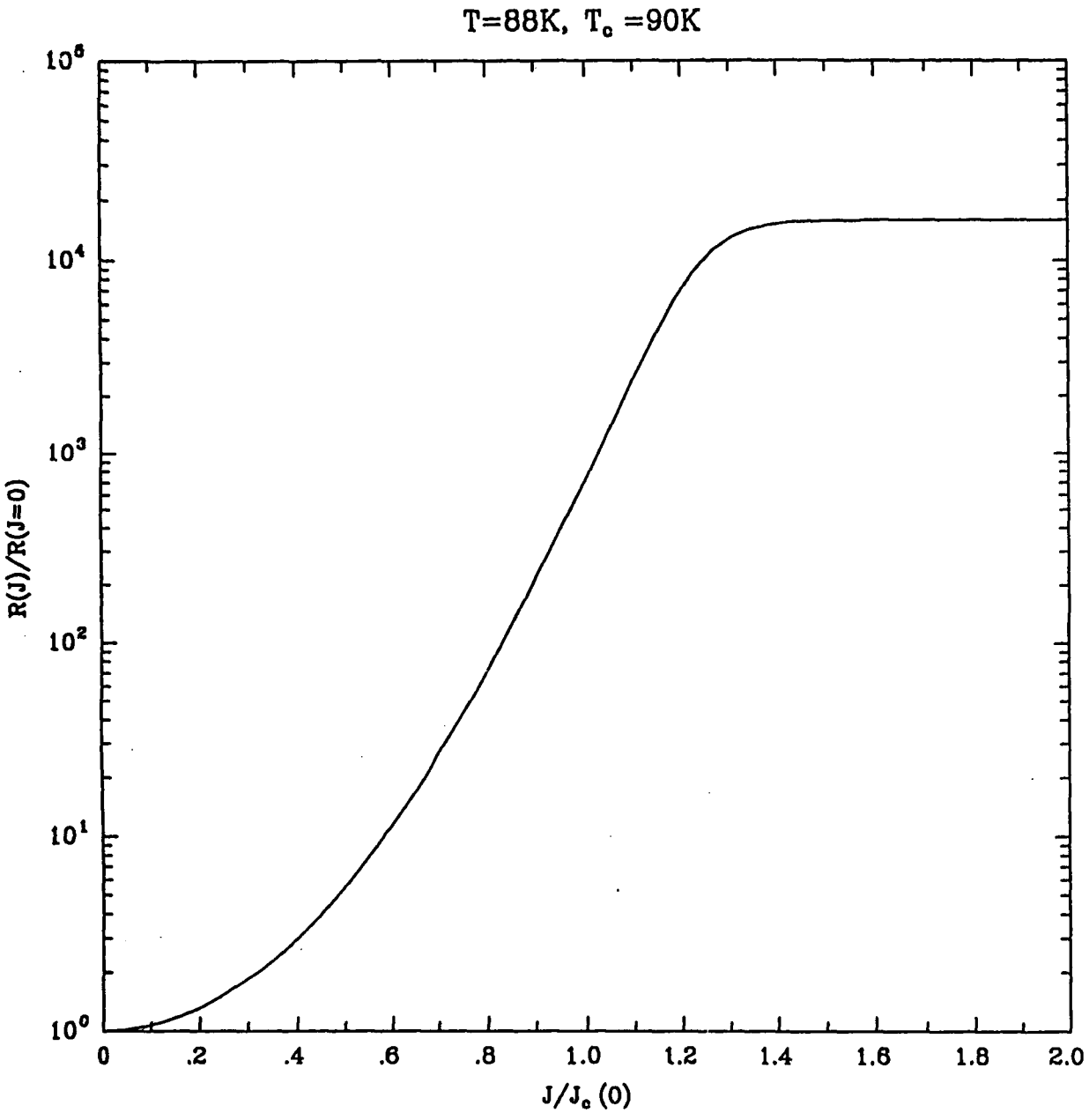
T=88K, T_c =90K
10^6
10^4
10^3
10^2
10^1
10^0
R(J)/R(J=0)
0
.2
.4
.6
.8
1.0
1.2
1.4
1.6
1.8
2.0
J/J_c (0)

Fig. 8a

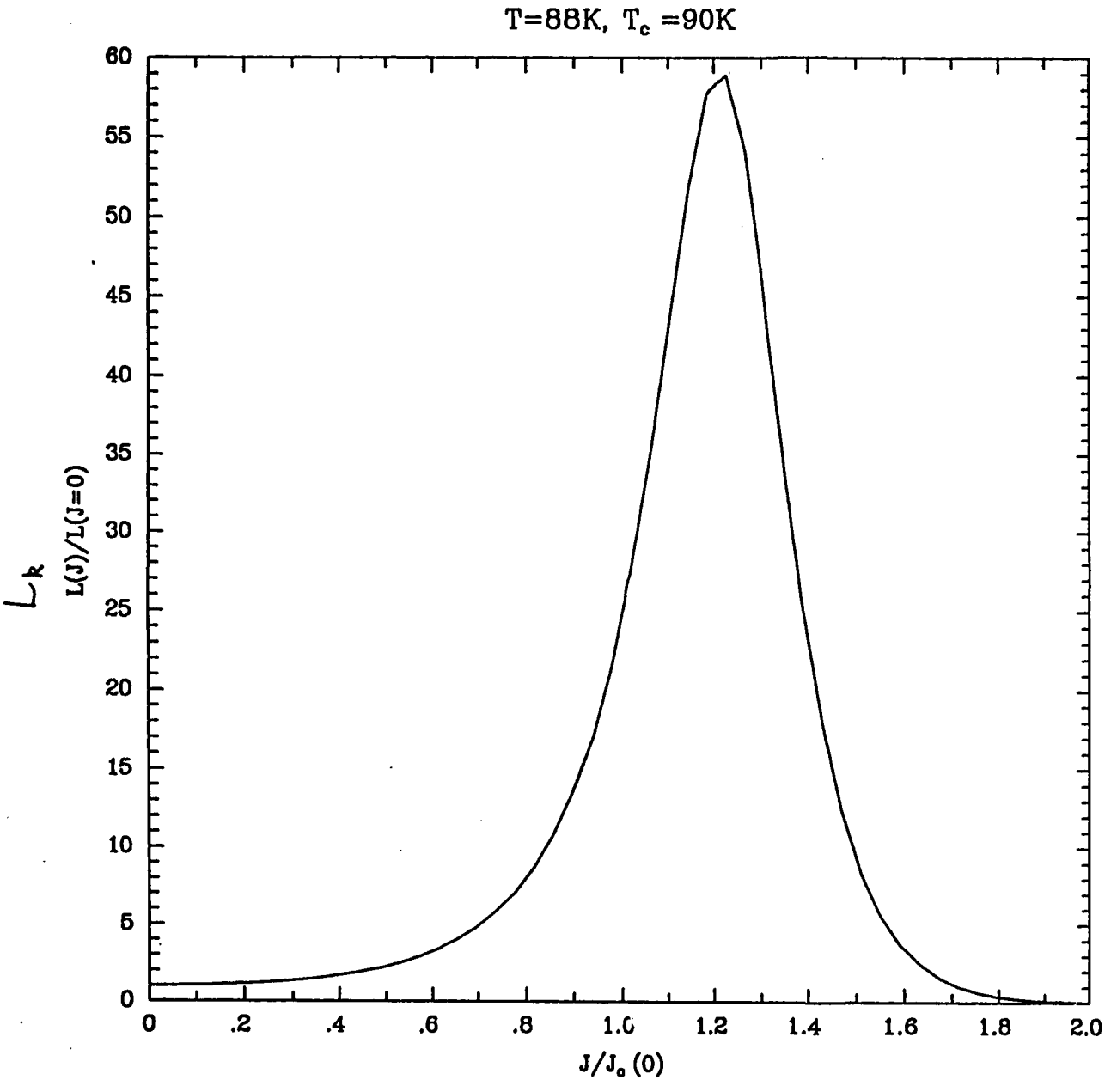
T=88K, T_c =90K
L_k
L(J)/L(J=0)
60
55
50
45
40
35
30
25
20
15
10
5
0
0
.2
.4
.6
.8
1.0
1.2
1.4
1.6
1.8
2.0
$J/J_o(0)$

Fig. 8b

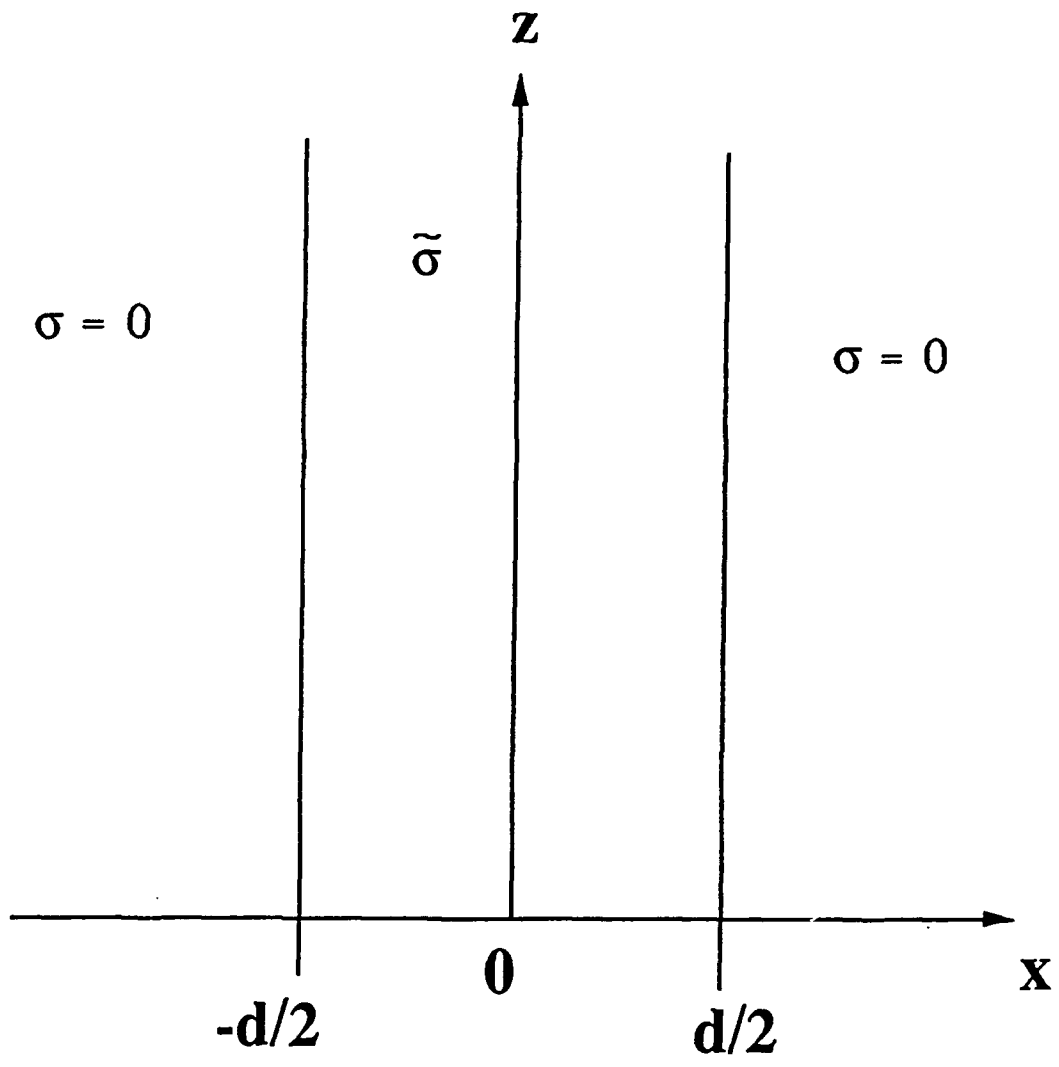

Fig. 9 A superconducting slab

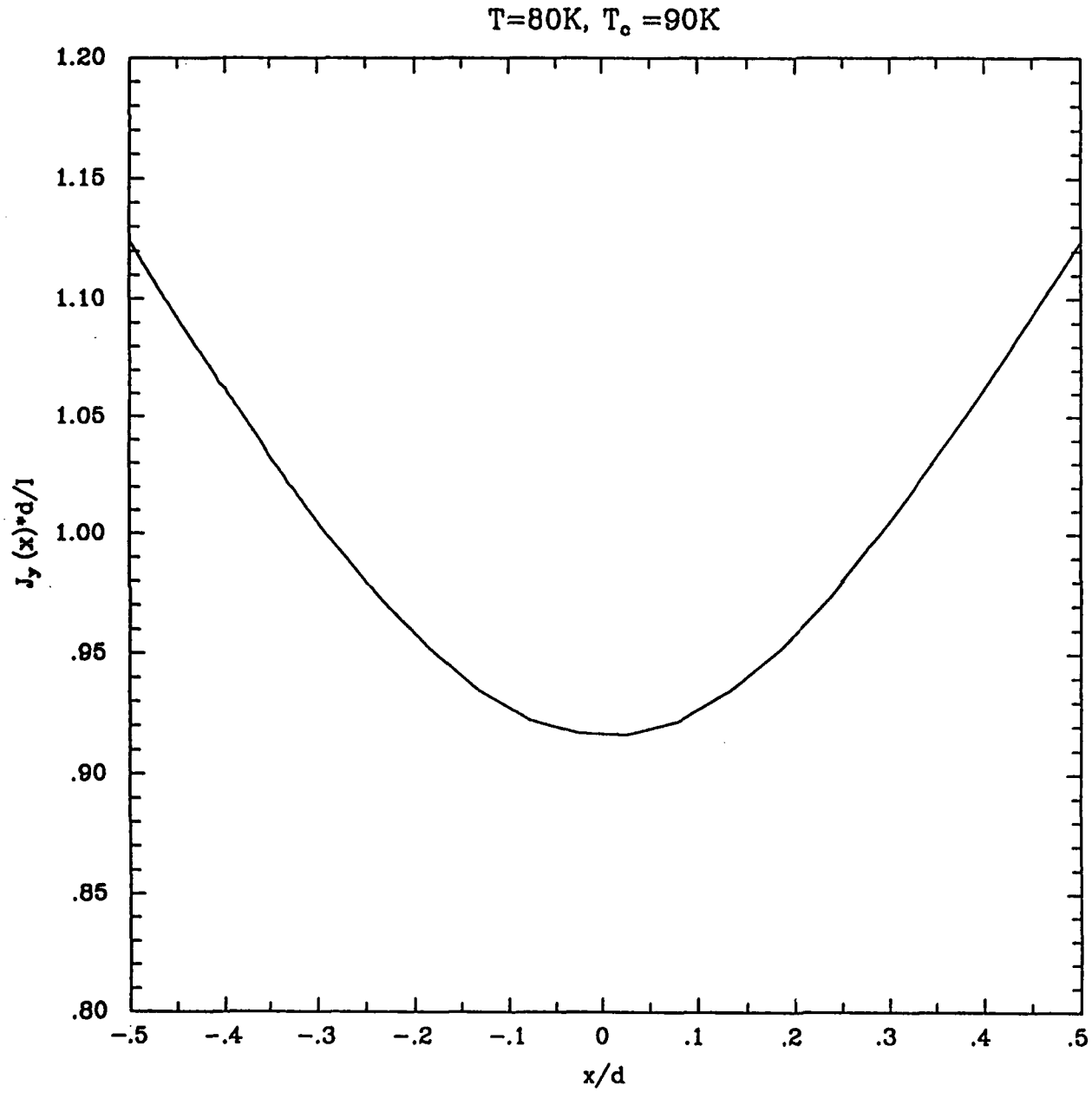
T=80K, T_c =90K
1.20
1.15
1.10
1.05
1.00
.95
.90
.85
.80
$J_y(x)*d/I$
−.5
−.4
−.3
−.2
−.1
0
.1
.2
.3
.4
.5
x/d

Fig. 10a

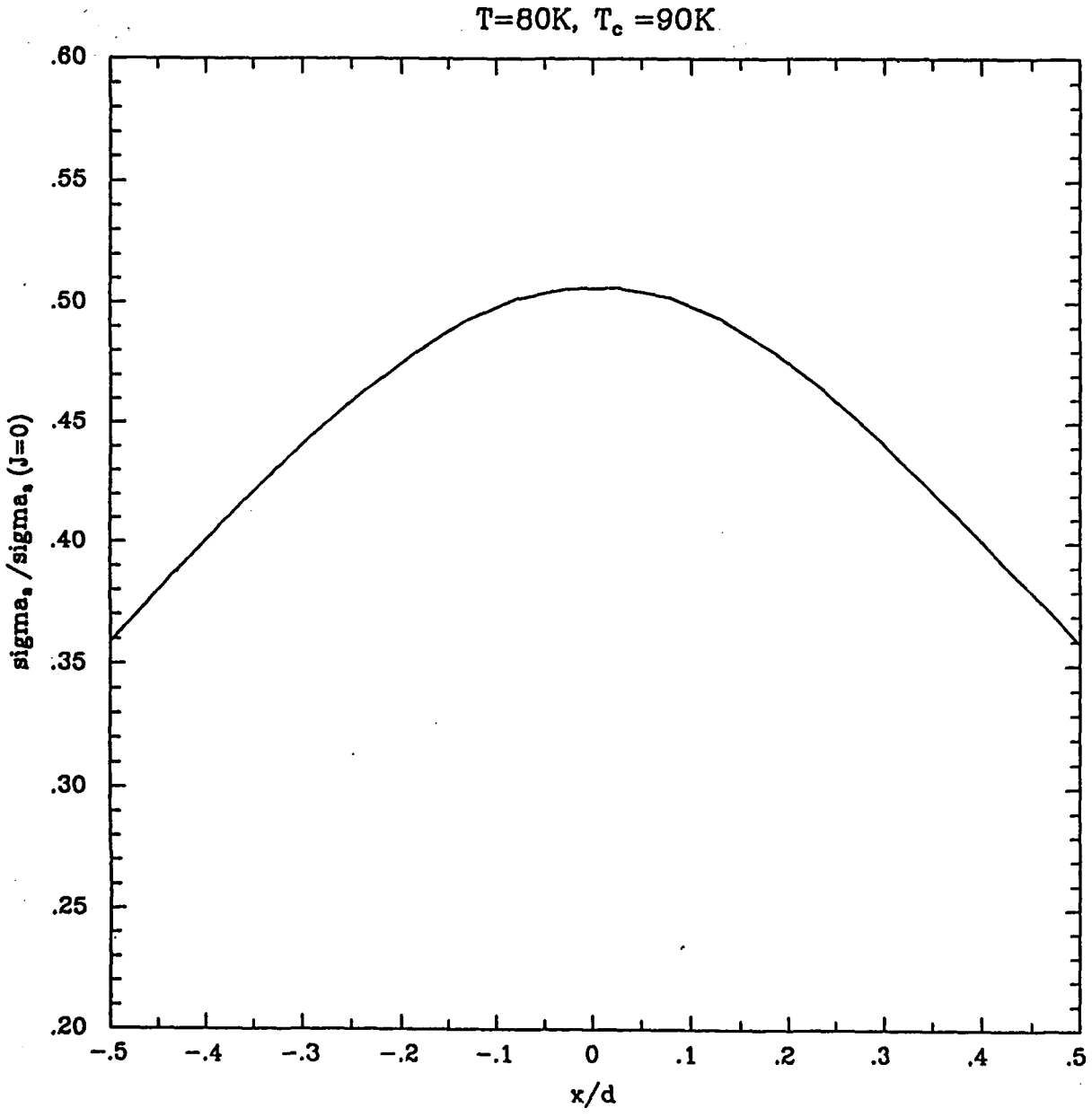
T=80K, T_c =90K
.60
.55
.50
.45
.40
.35
.30
.25
.20
sigma$_s$ /sigma$_s$ (J=0)
−.5
−.4
−.3
−.2
−.1
0
.1
.2
.3
.4
.5
x/d

Fig. 10b

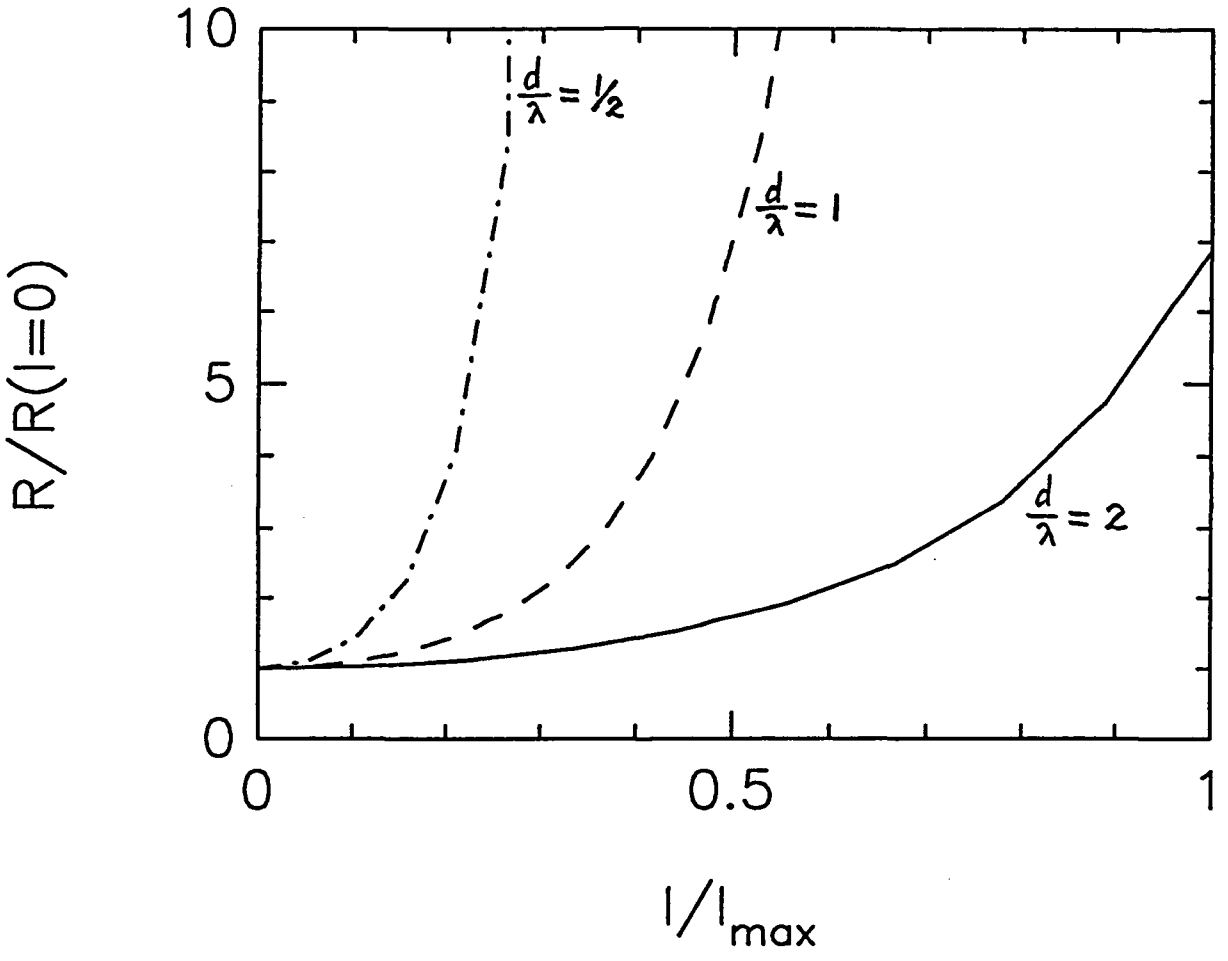

Fig. 11a

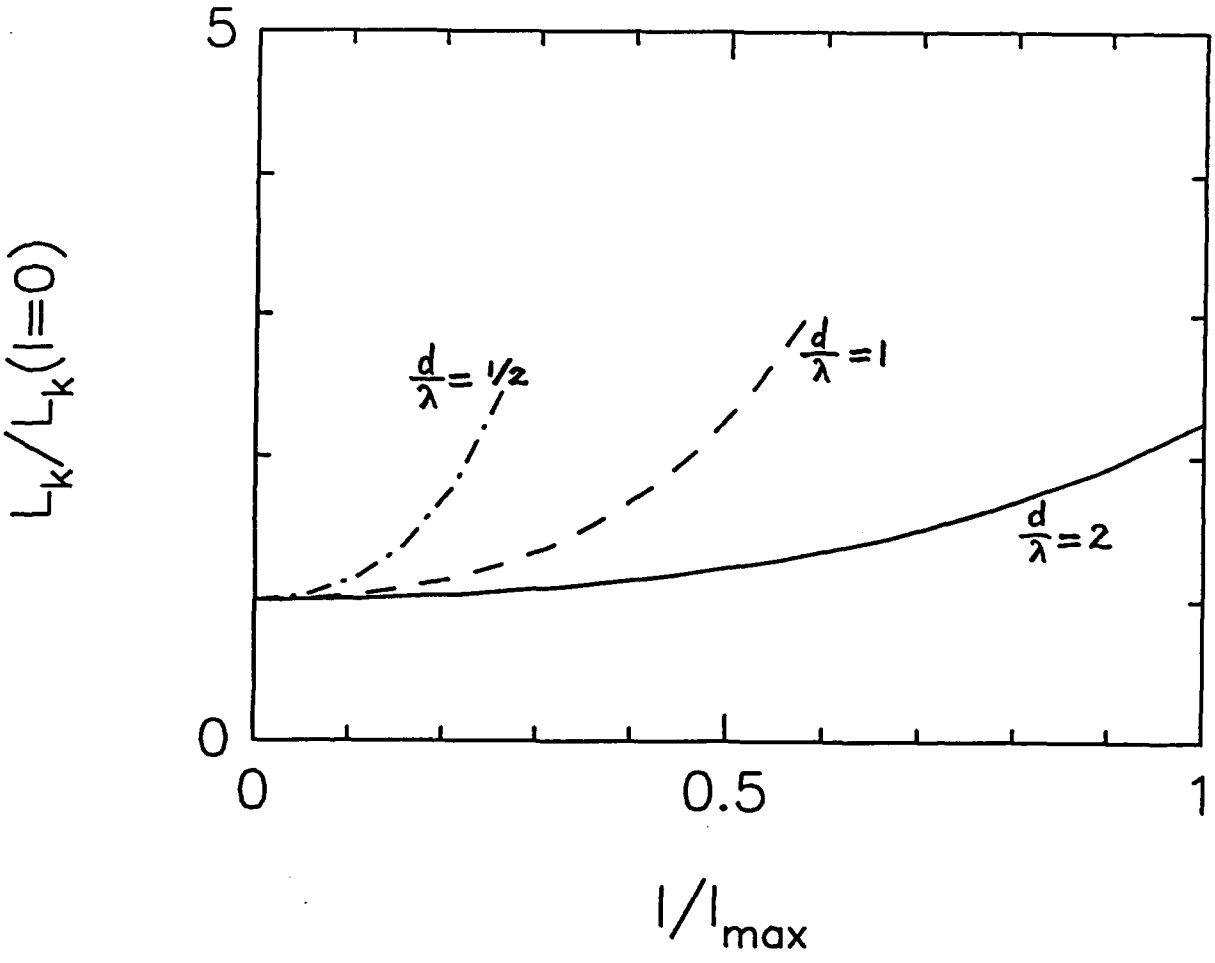
5
0
0
0.5
1
$L_k/L_k(I=0)$
I/I_{max}
$\frac{d}{\lambda}=1/2$
$\frac{d}{\lambda}=1$
$\frac{d}{\lambda}=2$

Fig. 11b

$T = 88K,\ T_c = 90K$

Surface Resistance.

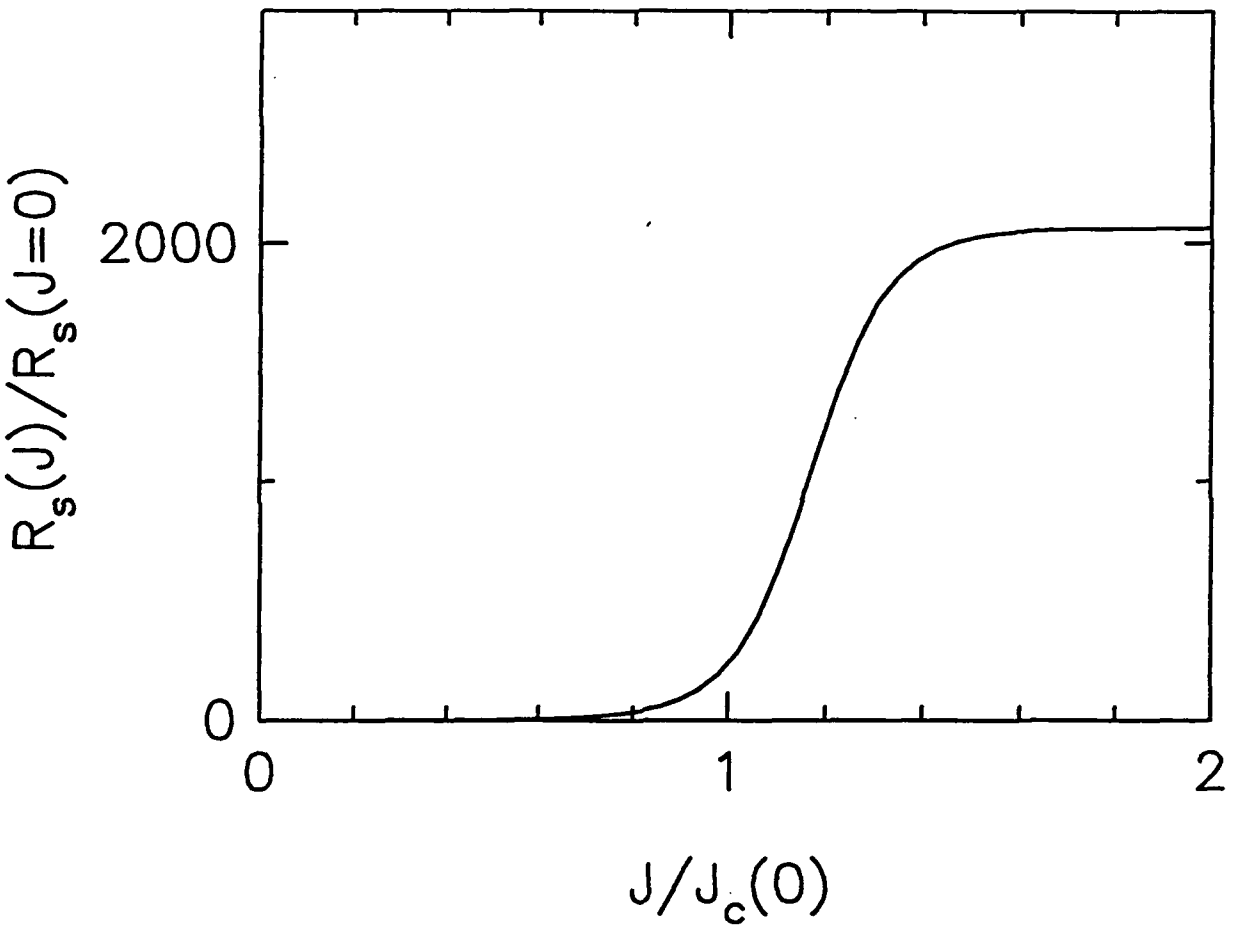

Fig. 12a

XIA 3-MAR-1992 20:44

$T = 88K$, $T_c = 90K$

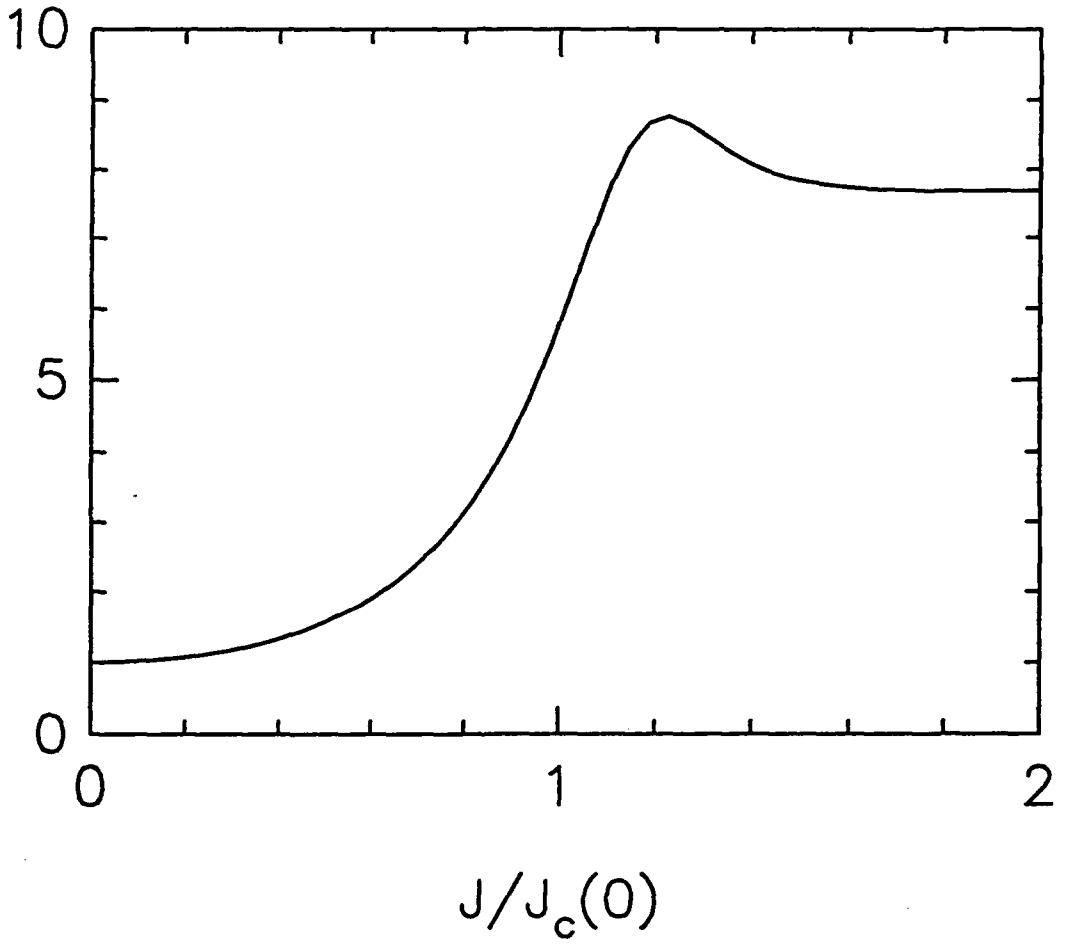

Fig. 12b

XIA 3-MAR-1992 20:47

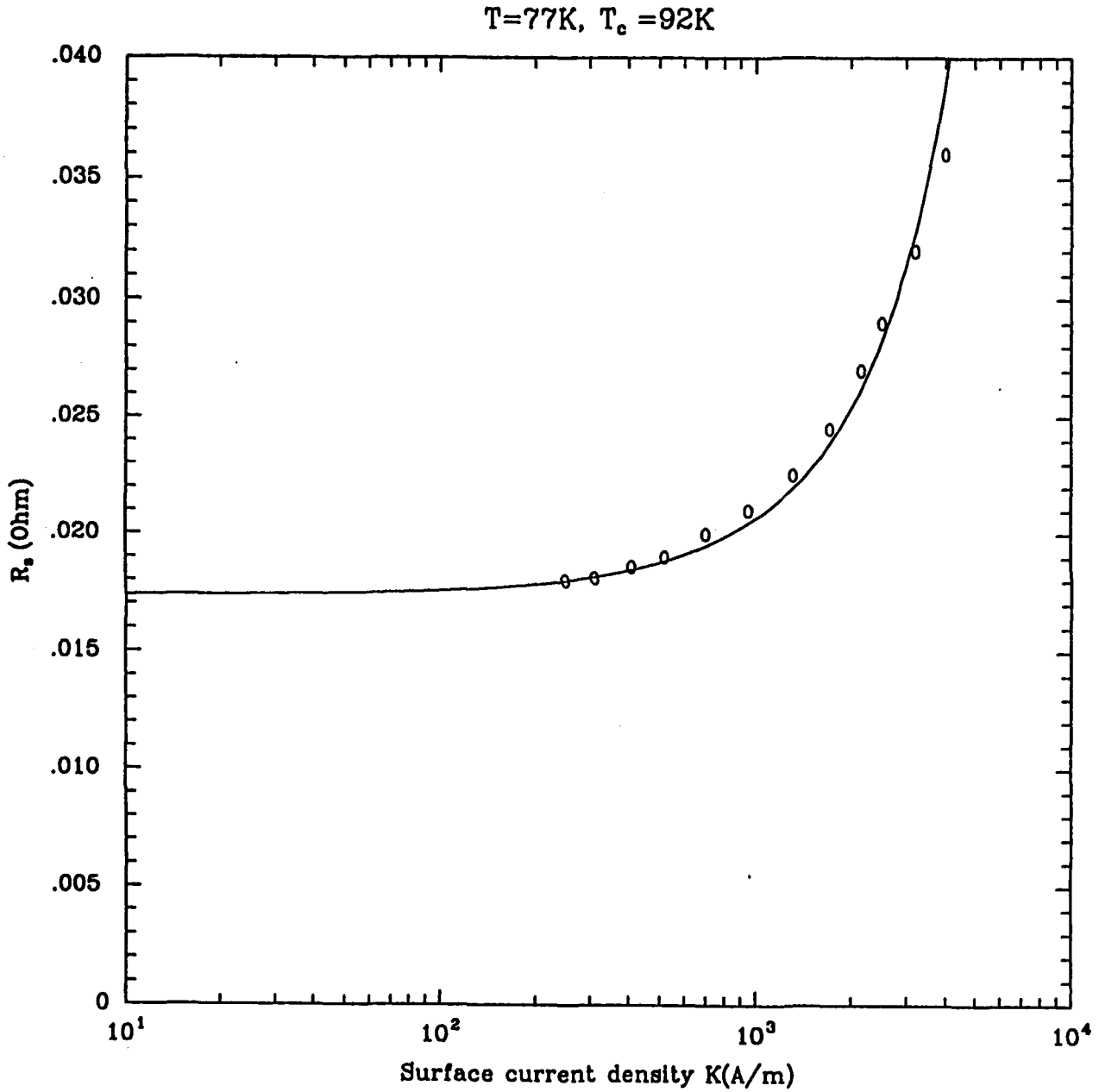
T=77K, T_c =92K
.040
.035
.030
.025
.020
.015
.010
.005
0
R_s (Ohm)
10^1
10^2
10^3
10^4
Surface current density K(A/m)

Fig. 12c

ELECTROMAGNETIC PROFILE RECONSTRUCTION USING THE RICCATI EQUATION APPROACH

Jiqing Xia *, Arthur K. Jordan +, Jin A. Kong

Department of Electrical Engineering and Computer Science

Massachusetts Institute of Technology, Cambridge, MA 02139

+ Permanent address: Center for Advanced Space Sensing

Naval Research Laboratory, Washington DC 20375

The Riccati differential equation for reflection coefficients in one-dimensional inhomogeneous media is applied to the electromagnetic inverse scattering problem. Two types of the Riccati equation in literature, Schelkunoff's and Redheffer's, are derived and distinguished. Based on inverting Redheffer's Riccati equation, both linear and non-linear inversion formulae are proposed. These renormalized perturbation formulae reconstruct the dielectric profile from the reflection coefficient at the surface of the medium. Existing inversion formulae (including the Born approximation) which were obtained from the Green's function approach and the Gel'fand-Levitan-Marchenko (GLM) theory are now derived from the Riccati equation. Four inversion schemes based on inverting the Riccati equation, linearized Redheffer's Riccati equation, linearized Schelkunoff's Riccati equation, non-linear Redheffer's Riccati equation and non-linear Schelkunoff's Riccati equation approaches, are used to invert several dielectric profiles. Comparison and summary of these methods are given. All these methods give higher order inversion results than the first-order Born approximation. The inversion is performed on band-limited reflection coefficients in frequency domain. An inverse Liouville transform is introduced to rigorously recover the geometric lengths from the stretched coordinates in the inversion procedure.

Electromagnetic Inverse Scattering In Remote Sensing

Jake J. Xia
Office 36-377
Department of Electrical Engineering and Computer Science
Massachusetts Institute of Technology
Cambridge, MA 02139
(617)-253-4186

Jin A. Kong
Office 26-305
Department of Electrical Engineering and Computer Science
Massachusetts Institute of Technology
Cambridge, MA 02139
(617)-253-5625

Inverting the physical parameters which usually appear as inhomogeneous profiles from measurements has been a challenging task for the remote sensing community. Due to complexity of the media, the forward problem in remote sensing of forest, vegetation and sea ice, typically in random media, has attracted researchers' efforts in the past two decades. Techniques which serve the ultimate goal of solving the inverse problem have also evolved and entered into a practical stage.

In general, the inverse methods can be summarized in three categories. The first one is a data base approach. Whenever a measurement result comes in, it will be compared with all the pre-stored patterns in a library to identify the possible targets. In industry, it is called data interpretation which strongly relies on previous experience. The accumulation of data in the library is a learning process. The advantage of this method is that the unknowns can be identified exactly if such target has been seen before so that the cause and the result are directly connected. The disadvantage is that if the data base is not big enough, the target can not be identified, or if the data base is too big, it will take too much time to search for and match the right pattern.

The second method is the iterative approach. A forward model of deducing results from causes has been established before the inversion. When a measurement is obtained, a set of guessed values for the unknowns will be put in the froward model as the possible causes. If the predicted result of the forward model does not match the measurement, an adjusted set of parameters will be used as a new guess. The whole procedure will be repeated until the match is found. During iterations, how to correct the error to reach fastest the convergent value is very important. This procedure is also called optimization or error minimization, which by itself is an active research area. Iterative methods are particularly useful when the solution of an integral equation can not be found in an explicit form. As an example of the iterative methods, the Born approximation approximates the forward model in a linearized form, then iterates towards convergence. The advantage of the iterative approach is that an accurate final solution can be found at a relative fast (compare to data base search) speed. The method is also flexible for different kinds of targets, unlike the data base search where the target has to have been seen before. The disadvantage is that the convergence of iteration is not always guaranteed. There are usually more than one minimum of the cost function. The initial guess is sometimes so critical to assure the right convergent result that *a priori* information needs to be used. Non-uniqueness is a serious problem in all inversion methods. Sufficient number of measurements are helpful of reducing the degree of non-uniqueness. Formulation of the forward model for the final inversion equation determines how efficient the inversion scheme is, which sometimes also affect the degree of non-uniqueness.

A recently developed inversion method referred to as the renormalized Source-Type Integral Equation (STIE) approach [1] solves the integral equation derived from the Green's function [2] without the linear approximation. The STIE approach formulates an exact forward model, hence is not restricted to low contrast profiles or weak scattering. The STIE method has been applied to profile inversion problems of the soil moisture [3] and oil formation in boreholes [4], where the medium properties are described by the permittivity and conductivity distributions. The unknown profiles are inverted from the electromagnetic measurements at remote observation points.

The third category of inverse methods is the explicit solution approach. When one solves the inversion equation, closed-form solutions may be obtained if the problem is formulated in certain ways and the data is in certain forms. Examples of this method include the Gel'fand-Levitan-Marchenko (GLM) theory when rational reflection coefficient is used and methods of inverting the Riccati equation [5]. The advantage is obviously that the convergence is guaranteed and the speed is excellent. Unfortunately, only a very few practical problems can be solved by

using this method. It is usually used as a check for other inversion methods or for mathematical studies.

In this paper, we will review the above inverse methods with our focus on iterative methods, especially the STIE approach. The STIE approach is extended to the case of a general background medium. The formulation of the inversion equation is exact. Numerical optimization methods are employed in the solution of the inversion equation. The inversion equation also has an explicit dependence on the unknowns to be inverted for; this allows one to compute the derivatives (including higher orders) of the response with respect to these unknowns in a closed form. Therefore, higher-order convergence can be achieved without increasing much of the computational time. By pre-storing the elements of the inversion equation (which depend only on the background medium and are independent of the unknown profile), the method does not require the solution to the full forward problem repeatedly as in the case of the Distorted Born approach and is therefore faster in implementation. An algorithm is formulated for simultaneously inverting the unknown permittivity and conductivity profiles. As an example, a soil moisture profile is inverted from measurements above the ground.

References

[1] Habashy, T.M., E.Y. Chow and D.G. Dudley, "Profile inversion using the renormalized source type integral equation approach", IEEE Trans. on Antenna and Propagation, vol. AP-38, pp.668-682, May, 1990.

[2] J. A. Kong, "Electromagnetic Wave Theory," John Wiley & Sons, Inc., Ch.3, second edition, 1990.

[3] J. Xia, T.M. Habashy, R.T. Shin and J.A. Kong, "The renormalized STIE approach applied to inversion of soil moisture profiles", IEEE URSI National Radio Science Meeting, Boulder, Colorado, Jan. 1992.

[4] J. Xia, T.M. Habashy and J.A. Kong, "Profile inversion in a cylindrically stratified lossy medium using the source-type integral equation approach", presented at Progress In Electromagnetics Research Symposium, Cambridge, July 1991.

[5] J. Xia, A.K. Jordan and J.A. Kong, "Profile reconstruction based on the Riccati equation", submitted to Journal of Optical Society of America (A).

Office of Naval Research

DISTRIBUTION LIST

Arthur K. Jordan

Code: 1114SE
Office of Naval Research
800 North Quincy Street
Arlington, VA 22217

3 copies

Administrative Contracting Officer
E19-628
Massachusetts Institute of Technology
Cambridge, MA 02139

1 copy

Director
Naval Research Laboratory
Washington, DC 20375
Attn: Code 2627

6 copies

Defense Technical Information Center
Bldg. 5, Cameron Station
Alexandria, VA 22314

2 copies